ULg Library

http://lib.ulg.ac.be

http://matheo.ulg.ac.be

Contribution to the development of a microphotoreactor for the production of pharmaceutical compounds

Auteur : Palm, Guillaume
Promoteur(s) : Heinrichs, Benoit
Faculté : Faculté des Sciences appliquées
Diplôme : Master en ingénieur civil en chimie et science des matériaux, à finalité spécialisée
Année académique : 2016-2017
URI/URL : http://hdl.handle.net/2268.2/2579

Avertissement à l'attention des usagers :

Tous les documents placés en accès ouvert sur le site le site MatheO sont protégés par le droit d'auteur. Conformément aux principes énoncés par la "Budapest Open Access Initiative"(BOAI, 2002), l'utilisateur du site peut lire, télécharger, copier, transmettre, imprimer, chercher ou faire un lien vers le texte intégral de ces documents, les disséquer pour les indexer, s'en servir de données pour un logiciel, ou s'en servir à toute autre fin légale (ou prévue par la réglementation relative au droit d'auteur). Toute utilisation du document à des fins commerciales est strictement interdite.

Par ailleurs, l'utilisateur s'engage à respecter les droits moraux de l'auteur, principalement le droit à l'intégrité de l'oeuvre et le droit de paternité et ce dans toute utilisation que l'utilisateur entreprend. Ainsi, à titre d'exemple, lorsqu'il reproduira un document par extrait ou dans son intégralité, l'utilisateur citera de manière complète les sources telles que mentionnées ci-dessus. Toute utilisation non explicitement autorisée ci-avant (telle que par exemple, la modification du document ou son résumé) nécessite l'autorisation préalable et expresse des auteurs ou de leurs ayants droit.

UNIVERSITY OF LIEGE
FACULTY OF APPLIED SCIENCE

Contribution to the development of a microphotoreactor for the production of pharmaceutical compounds

Guillaume PALM

Thesis presented for obtaining the Master's degree in:
Chemical and Materials engineering

Supervisor:
Benoît Heinrichs

Co-Supervisor:
Jean-Christophe Monbaliu

Academic year: **2016 – 2017**

Acknowledgements

I would first like to thank Professor Benoît Heinrichs, promotor of this work, and Dr. Jean-Christophe Monbaliu, co-promoter of this work, who gave me the opportunity to join the icFlow project and perform my Master Thesis in their Labs. I would also like to thanks them for the follow-up of my work.

In particular, I would also like to thank PhD student Carlos Mendoza for his coaching, his help in the theoretical and practical fields, and his availability all along this work.

My thank goes also to all the other members of the icFlow project, Professor Laurent Dreesen, Dr. Carlos Paéz, and PhD student Noémie Emmanuel for the collaboration all along this project.

I would also like to thanks all the members of the department of chemical engineering and all the members of the CiTOS lab for all the moment shared during this year and the precious advices that I got all along the year.

Finally, I would like to thank Professor Dominique Toye and M. Jérome Jacq for agreeing to form the jury of my work.

Abstract - English

The aim of this work is to optimize the photooxygenation reaction of methionine (Met) into methionine sulfoxide (MetO) using microreactors. This requires the photosensitization of a dye for the production of singlet oxygen ($^1O_2$). The photosensitizer chosen was Rose Bengal (RB) coupled to silica nanoparticles (SiO_2 NPs). Different ways of using these NPs have been tested. They have been trapped in a TiO_2 matrix and coated on a glass slide of a mesoreactor, but have also been injected as a slurry in the microreactor. The first option did not work well due to the constant light exposition of the photosensitizer which can be rapidly degraded. Different silica particles have been synthetized and characterized: dense, mesoporous and microporous. The mesoporous particles have shown the most promising results because of their large surface area and sufficient pore volume. Two different coupling agents, EDC and HATU, have been tested, leading to slightly different final particles. EDC showed slightly better performances regarding conversion, but particles coupled by HATU turned out to be much more stable. Kinetic constants could be determined thanks to the plug flow reactor model. Finally, different parameters were tested in the microreactor, and the resulting conclusions indicated that a low liquid flowrate, working at high pressure, and low concentrations of RB, were founded as optimal conditions.

Résumé – Français

Le but de ce travail est d'optimiser la réaction de photooxygenation de la méthionine (Met) en méthionine sulfoxide (MetO) en utilisant un microréacteur. Cela requière l'excitation photonique d'un photosensibilisateur afin de produire de l'oxygène singulet ($^1O_2$). Le photosensibilisateur choisi est le Rose Bengale (RB) couplé à des nanoparticules de silice (SiO_2 NPs). Différentes façon d'utiliser ces particules ont été testées. Elles ont été incorporées dans une matrice de TiO_2 qui a été revêtu sur des lames de verre utilisés avec un mesoréacteur, mais elles ont aussi été injectées en suspension dans un microreacteur. La première option n'a pas donné satisfaction du à l'exposition permanente à la lumière du photosensibilisateur qui fût dégradé rapidement. Différentes particules de silice ont été synthétisées et caractérisées : Des particules denses, mesoporeuses and microporeuses. Les particules mesoporeuses ont montré les résultats les plus prometteurs, dus à leur grande surface et un volume de pore suffisant. 2 agents de couplages différents, EDC et HATU, ont été testés, conduisant à des particules légèrement différentes. EDC a montré des performances légèrement meilleures en ce qui concerne la conversion, mais les particules couplées avec l'HATU se sont montrées être beaucoup plus stables. Des constantes cinétiques ont pu être déterminées grâce au modèle du réacteur piston. Enfin, différents paramètres ont été testés avec le microréacteur, et les conclusions résultantes sont que de faibles débits liquides, travailler à haute pression, and à faible concentration de RB, sont les conditions optimales.

Table of Contents

0. List of abbreviations 6

1. Introduction 7

2. Synthesis of Nanoparticles and coating 15

2.1 TiO_2-SiO_2-RB coating for the mesoreactor 15

2.2 Mesoporous SiO_2-RB Nanoparticles 19

2.3 Direct amino-functionalized SiO_2-RB Nanoparticles 21

3. Characterization of the particles 22

3.1 Thermogravimetric (Tg) analysis 22

3.2 Profilometry 26

3.3 BET isotherms, BET Surface area, and BJH desorption Pore volume 27

3.3.1 Dense nanoparticles 28

3.3.2 Mesoporous nanoparticles 29

3.3.3 Microporous particles 30

3.3.4 Summary 31

3.4 UV-visible spectrum 32

4. Mesoreactor and Microreactor 34

4.1 Mesoreactor 34

4.2 Microreactor 37

4.3 Light source characterization 39

4.4 Solvent choice 41

5. Results 43

5.1 Mesoreactor 43

5.1.1 Test 1 43

5.1.2 Test 2 43

5.1.3 Test 3 44

5.1.4 Test 4 45

5.1.5 Summary and Conclusion 46

5.2 Microreactor 47

5.2.1 Series 1 – Variation of the reactor's length 48

5.2.2 Series 2 – Variation of the RB concentration 50

5.2.3 Series 3 – Variation of the liquid flowrate 53

5.2.4 Series 4 – Variation of the pressure 55

5.2.5 Summary and conclusion 58

6. Conclusion & perspectives 59

Bibliography..... 61

0. List of abbreviations

- Singlet oxygen: $^1O_2$
- Rose Bengal: RB
- Silica: SiO_2
- Nanoparticles: NPs
- Methionine: Met
- Methionine sulfoxide: MetO
- Nuclear Magnetic Resonance: NMR

1. Introduction

The aim of this work is the optimization of the photooxygenation of L-methionine (Met) into L-methionine sulfoxide (MetO) (see Figure 1) in microreactors. The oxygenation was conducted through photocatalysis induced by Rose Bengal (RB) (see Figure 2) supported on silica nanoparticles (SiO_2 NPs) as photosensitizer.

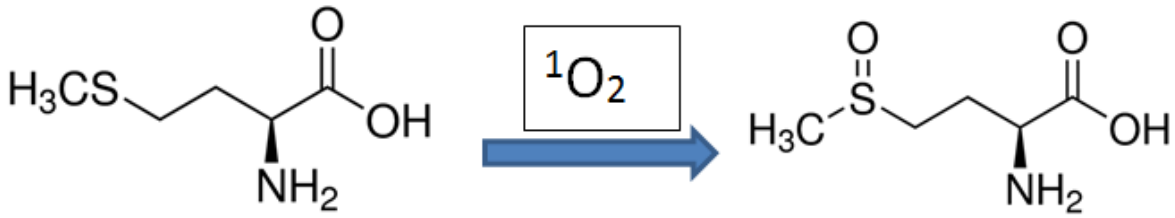

Figure 1. Oxygenation of L-Methionine into L-Methionine sulfoxide by singlet oxygen [1],[2]

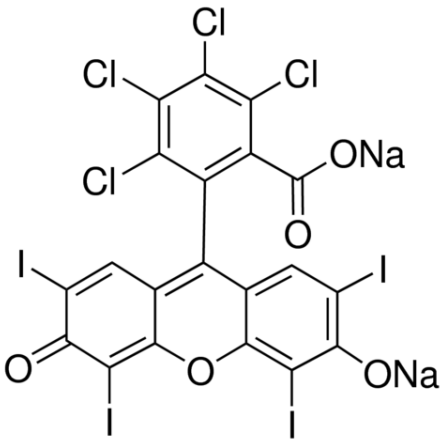

Figure 2. Rose Bengal (4,5,6,7-Tetrachloro-2',4',5',7'-tetraiodofluorescein disodium salt) [3]

The studied photooxygenation reaction relies on the excitation of oxygen in order to create singlet oxygen ($^1O_2$) the first excited state of oxygen [5]. This $^1O_2$ is generated by energy transfer from the excited photosensitizer to triplet oxygen (see Figure 3) [4]: The photosensitizer is irradiated at the appropriate wavelength to reach its excited state. In the case of RB the appropriate wavelength corresponds to the visible green light, in the 540-560 nm range. The excited photosensitizer then undergoes relaxation and loses a part of its energy in form of thermal energy to become in the triplet state. Finally there is an energy transfer between the photosensitizer that goes back to its ground state and the triplet oxygen that becomes excited $^1O_2$. The energy gap between the molecular oxygen's ground electronic state and the excited singlet state is of 94 kJ/mol [6]. This corresponds to a wavelength of 1273 nm. This means that $^1O_2$, if it does not react, reaches its ground state by emitting infrared light. The amount of $^1O_2$ produced depends on 3 major factors: The adsorption coefficient of the photosensitizer at the wavelength used, the triplet state energy, and the quantum

yield (~0,7 for RB) [7]. The quantum yield, in a photochemical process, is defined as the probability that an event occurs per photon adsorbed by the system [8]. In this case it therefore corresponds to the amount of $^1O_2$ produced in function of the adsorbed photons. Knowing that the quantum yield of RB is around 0,7 it means that when 10 photons are adsorbed by the system (10 molecules of the photosensitizer, RB, are excited), 7 molecules of $^1O_2$ are produced. In fact, what has the most interest in the work done is to optimize the production of $^1O_2$. The oxygenation reaction of the Met is an indicator of the quantity of $^1O_2$ produced.

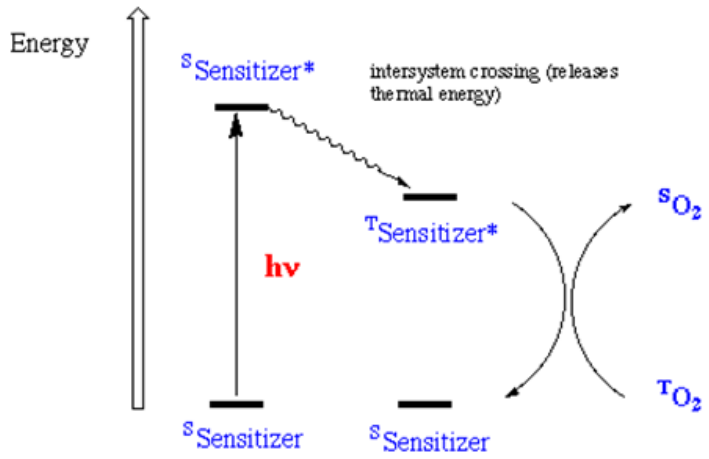

Figure 3. Production of singlet oxygen by photosensitization [9]

The accomplishment of this photooxygenation should bring the research one step forward into the field of photodynamic therapy, an innovative treatment for cancer: It consists in a light induced elimination of cancer cells and other drugs carriers. The high specificity of the photosensitizer should allow a localized photooxygenation and so a localized destruction of (cancer) cells [4].

In addition to the cancer photodynamic therapy, photosensitized production of $^1O_2$ is also applied in, sometimes complex, chemical synthesis [5], degradation of organic pollutants [10], inactivation of viruses, especially in water [10], photocarcinogenesis [6], and in the photodegradation of dyes and polymers [6]. In addition to the production of $^1O_2$, several research focus on the use of light energy instead of the classical thermal energy, because of the use of "green and sustainable" photons, and the fact that "free" sunlight energy reaches our planet every day [11]. In addition to that, working with light energy allows to work under mild conditions: the light activation of molecules doesn't require the use of high temperature to activate molecules in order to initiate reactions [11]. A typical example of the use of photochemistry is light catalyzed redox reactions: Light irradiates an organic dye or a transition metal that then converts the light energy carried by the photons into electrochemical potential. This potential then facilitates the electron transfer and so accelerates the redox reaction [11].

Another important parameter that has to be managed in photooxygenation is the toxicity of the photosensitizer [4]. To avoid the presence of RB in the final product, that could for instance avoid FDA approval when synthetizing drugs through photooxygenation, one main idea is investigated: immobilization. To achieve this 2 methods are available and both have been tested. Coupling the Rose Bengal to NPs that are then recovered through centrifugation of the final product, or immobilization of the photosensitizer on the walls of the reactor. The main drawback when

introducing the photosensitizer as a slurry and recovery through centrifugation is that, especially in microreactors, it could lead to clogging [11]. For this reason immobilization on the wall of the reactor is privileged. This however requires particular stable RB SiO_2 NPs for which bleaching is avoided or at least minimized. Immobilization or recovery of the particles has also a financial interest and can so increase the economic viability of the process [11].

The choice of the reaction, the oxygenation of Met, is based on 2 main criteria: First of all the high reaction selectivity: There is only one product formed during the oxygenation of Met, the MetO. Secondly the ease of characterization of the reaction: By performing proton Nuclear Magnetic Resonance (H-NMR) it is easy to differentiate the Met and MetO that have peaks at different chemical shifts which allows an easy calculation of the conversion: For the Met, the 2 protons attached to the carbon on the α-position of the sulfur have a chemical shift of 2,55. For the MetO, the 3 protons of the methyl group, on the α-position of the sulfinyl group have a shift of 2,65.

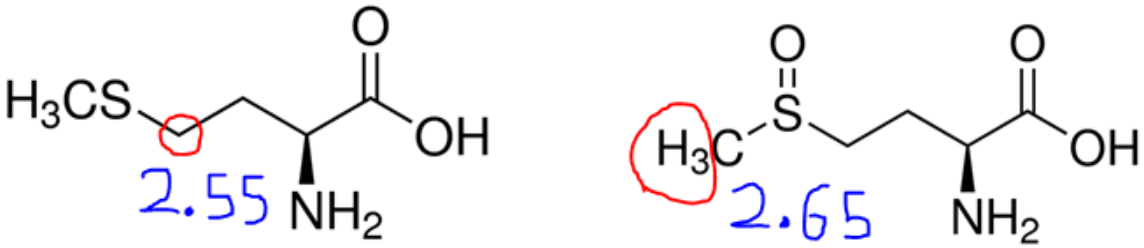

Figure 4. Chemical shifts and positions of the protons studied by RMN for the methionine and methionine sulfoxide [1], [2]

Oxygenation involving $^1O_2$ has several advantages: It has a high efficiency; easy working conditions ($^1O_2$ can be generated through a basic photosensitizer, oxygen that can come from air, and visible light, that can be basic sun light); and the reaction can take place in water, which avoids the use of organic solvents [5]. In general, the reactions involving $^1O_2$ are selective which allows skipping protection steps of sensitive functions that would be required by traditional oxidation [5]. The selectivity is due to the fact that the electrophilic $^1O_2$ preferentially oxidizes electron-rich sites like olefins, dienes, sulfides or aromatic compounds [10]. The high electrophilicity of $^1O_2$ even allows reaction that would not occurs with molecular oxygen [11]. All these positive effects lead to the fact that reactions can be conducted under mild conditions (i.e. room temperature) [12].

Nevertheless $^1O_2$ has also a major disadvantage: Its lifetime is strongly solvent dependent and usually really short [12]: 3.1-4.2 µs in water [6]. This leads to a low concentration of $^1O_2$ in the system.

Several studies have demonstrated that by coupling the photosensitizer to NPs, some advantages could be obtained, like for example protection of the photosensitizer or control of the distance between a metal and the photosensitizer in the case of core-shell immobilization. For this reason different types of SiO_2 NPs (dense and mesoporous) were synthetized in this work by different ways. These NPs were functionalized with APTES ((3-Aminopropyl)triethoxysilane) (see Figure 5) in order to obtain some amino groups on the SiO_2 NPs. RB was then attached to these amino groups on the NPs by two coupling agents: EDC (N-(3-Dimethylaminopropyl)-N'-ethylcarbodiimide hydrochloride) (see Figure 6) and HATU (1-[Bis(dimethylamino)methylene]-1H-1,2,3-triazolo[4,5-b]pyridinium 3-oxid hexafluorophosphate) (see Figure 7).

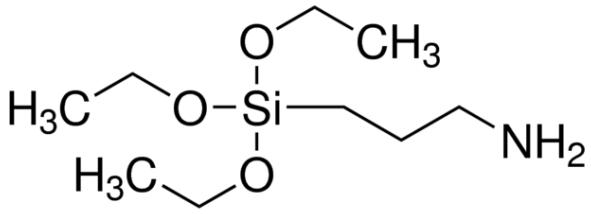

Figure 5. APTES / (3-Aminopropyl)triethoxysilane [13]

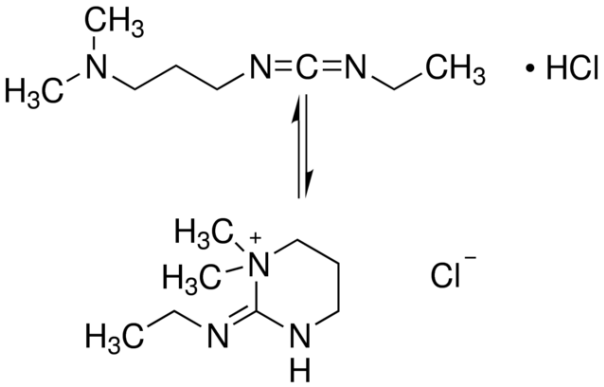

Figure 6. EDC / N-(3-Dimethylaminopropyl)-N'-ethylcarbodiimide hydrochloride [14]

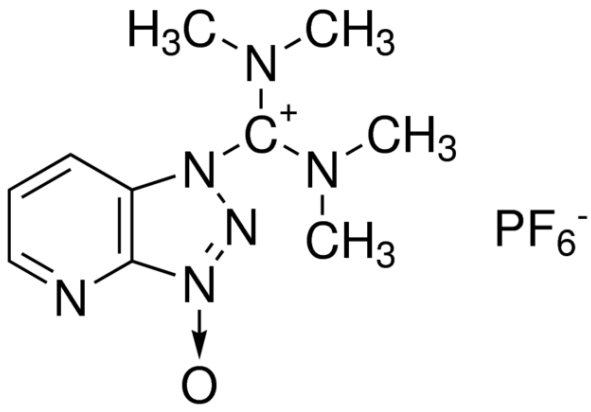

Figure 7. HATU / 1-[Bis(dimethylamino)methylene]-1H-1,2,3-triazolo[4,5-b]pyridinium 3-oxid hexafluorophosphate [15]

For the reaction studied, the main advantage of working with continuous meso/micro reactors compared to batch reactors is that the main drawback of using photochemistry is solved: the light penetration [11]. For the batch reactor, especially for concentrated solutions and common photosensitizer or organic dyes, which are strong absorbers [11], the light only penetrates some cm or mm and so doesn't reach the center of the reactor which leads to a loss of efficiency of the reactor (see Figure 8). This phenomenon is due to the exponential decrease of light transmission with the length of the sample. It can be avoided or at least limited by using thin sample lengths, and exactly this is the case with our meso-reactor which thickness is 1 mm or with the micro-reactor that consists of 800µm diameter tubing. The fundamental difference between microreactors and mesoreactors are their lateral dimensions and their inner volume: While the microreactors have lateral dimensions smaller than 1 mm and a volume between 1 µL and 10 mL, the mesoreactors have internal channels larger than 1 mm and a volume of several tens of mL [16].

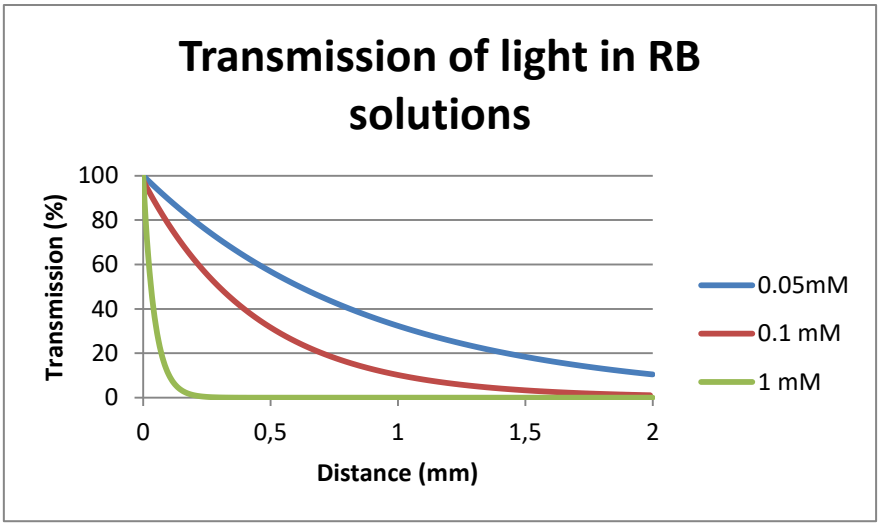

Figure 8. Transmission of light as a function of the distance for different concentration of Rose Bengal solutions (0.05 mM, 0.1 mM, 1 mm). The extinction coefficient of Rose Bengal is provided by Sigma-Aldrich ε=98000 $M^{-1}cm^{-1}$ and is valid between 546 and 550 nm light wavelength [3].

Also of great importance is the better heat and mass transfer due to greater interfacial areas (Figure 9) resulting from enhanced surface-to-volume ratio [12]: Especially in the case of oxygenation of Met is the huge interfacial area, between liquid and gas phase, of high importance. It allows maximizing the mass transfer of oxygen into the liquid and so increasing the kinetic of the reaction. Concerning the heat transfer it has a huge importance because it allows keeping the temperature inside the reactor stable and so avoids the formation of byproducts [11]. The use of LEDs, that doesn't not produce a lot of heat help to further stabilize the temperature in contrast to the use of a halogen lamp that requires cooling.

Figure 9. Microreactor system used: 4m long and composed of a 800 µm diameter tubing (PFA)

Another important factor in microreactors is a much easier scale-up: To do so, 3 options are available. The first consist in increasing simultaneously the flowrate and the length of the reactor resulting in identical residence time but with increased production. This increased flowrate will even affect positively the hydrodynamics of the flow by providing better heat and mass transfer [12]. The drawback of this solution is that an increased length of reactor leads to a higher pressure drop between the input and the output of the reactor and so also increased energy dissipation [11]. The second and third options are called internal and external numbering-up. Numbering-up consists in multiplying the number of reactors and to put them in parallel. This kind of scaling up is much easier than modifying the geometry of the reactor that often, in addition to the light penetration issue discussed above (see Figure 8), leads to different hydrodynamic behaviors and so to different performances. For the external numbering-up, each reactor has its own equipment (e.g. pumping system, process control, and so one) while for the internal numbering-up the equipment is common for all the reactors [12]. Both methods have advantages and drawbacks: Advantages of the external numbering-up are that individually failures of reactors don't affect the rest of the reactor system, while the major drawback is the economically cost of all the equipment needed for each reactor. For the internal numbering-up the cost, especially for a high number of reactors in parallel, is a huge advantage but the drawback is the product and conversion distribution coming out of each reactor that can differ because of different pressure drops, flow rates (especially in the case of biphasic mixtures, like in our case, it is not easy to get equal flow rates distribution in each of the parallel micro-reactors [12]), or other parameters that can influence the reaction in each reactor [11].

The other advantages of working with continuous microreactors are obviously the possibility to work under continuous regime, but also a better control of the reaction and flow conditions [12], an improved safety by, on one side avoiding the hold-up of large amounts of potentially hazardous reagents and/or products inside of the reactor, and on the other side avoiding hot spots through excellent heat transfer [12], a high selectivity and reproducibility, once again because of excellent heat, mass and (in the case of photochemical reactions) photon transfer [11], and a faster, cleaner and intensified reaction. Also the much faster mixing in microreactors, typically 10 milliseconds, compared to the 20 seconds needed for a round-bottom flask reactor of 250 ml (with agitator of 2.5 cm at 500 rpm) is a capital strength [16]. All these strengths demonstrate that the micro-reactors have a bright and promising future.

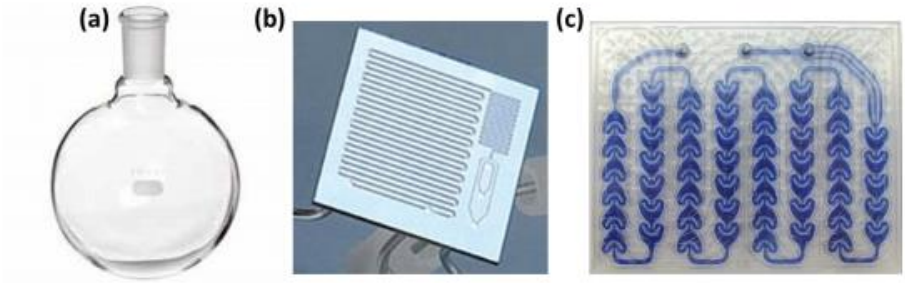

	Batch reactors	Continuous-Flow micro/mesoreactors
KEY FEATURES	3D internal structure >> 10^4 µm (typ. mL < internal volume < kL) Scale-dependent processes Low S/V ratio	3D internal structures < 1000 µm (typ. µL < internal volume < mL) Scale-independent processes High S/V ratio

Figure 10. Comparison between the batch reactors (a) and the meso/micro reactors (b) and (c) [16]

The choice of the material of the micro-reactor, PFA, a fluoropolymer (see Figure 11), has some advantages and some drawbacks: The most important advantages in this case are the low cost, the high flexibility that allows wrapping the tubing around a glass cylinder, and, the most important, it is transparent to light (UV & visible light) [12]. Other advantages are the excellent resistance to acidic and alkaline condition, especially at low and moderate temperature [12], and commercial availability [11]. One major drawback is the low thermal conductivity of the PFA that could slow down the heat removal [12]. Nevertheless, like mentioned above, the surface-to-volume ratio is so important that it does not have a great importance and the reactor can be considered as isothermal. Other drawbacks, but not so important in this case, are the low resistance to high temperatures [12] and degradation after prolonged UV radiations [11].

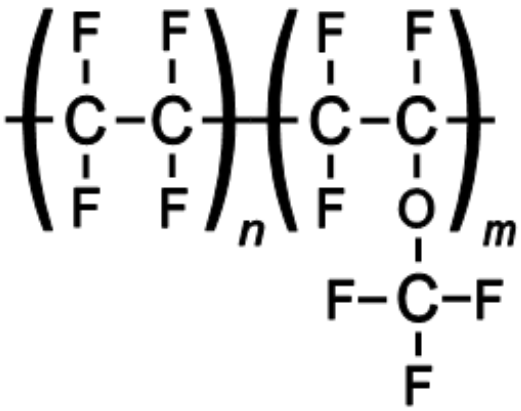

Figure 11. PFA / Perfluoroalkoxy alkane structure [17]

The micro-reactor, in the studied case, can easily be described as an isothermal plug flow reactor for following reasons: Because of the biphasic mixture, the liquid segments, of small size

compared to the entire reactor, are separated by gaseous segments. This leads to negligible axial dispersion: The only axial dispersion can occurs through the really thin, in our case negligible, liquid film along the walls of the reactor. Additionally, because of the slip velocity along the walls and the interfacial friction mixing occurs inside of the segments which allow considering them as perfectly mixed [12]. This corresponds perfectly to the definition of plug-flow reactors: no axial dispersion and infinite radial dispersion. Finally, because of the excellent heat transfer and dissipation due to the high surface-to-volume ratio, the reactor can, despite the heating from the light source and the exothermic reaction, be considered as isothermal [11].

2. Synthesis of Nanoparticles and coating

2.1 TiO_2-SiO_2-RB coating for the mesoreactor

These NPs were synthetized by drawing inspiration from the Stöber process [18]. This method allows the synthesis of dense SiO_2 NPs which were then dispersed in a TiO_2 matrix. This Sol-gel was then attached on glass slides via dip-coating. Finally, the slides were functionalized with Rose Bengal (RB).

Size and shape of NPs plays an important role in their properties. The Stöber process gives relatively spherical, amorphous, and homogeneous particles with a narrow size distribution. Their size can be adjusted by reaction condition, mainly with the TEOS concentration but also with the water and ammonia concentrations, the used solvent, reaction temperature, and pH [19]. Nevertheless, this work does not focus on the optimization of the Stöber synthesis and only one method, which had been previously optimized by other project participants, was used for the synthesis.

The SiO_2 NPs were synthetized by adding together, in the following order: 120 mL of ethanol (EtOH), 10 mL of aqueous ammonia (NH_4OH, ~25% w/w), 5 mL of Tetraethyl orthosilicate (TEOS, Figure 12) and 7,2 mL of deionized water (H_2O). The solution was stirred, at ambient temperature, during 90 minutes. The reaction that is taking part here is the hydrolysis of the TEOS followed by a condensation to form the SiO_2 NPs (The mechanism is shown in Figure 13). The ammonia plays the key role of catalyst in the hydrolysis and condensation reactions [18].

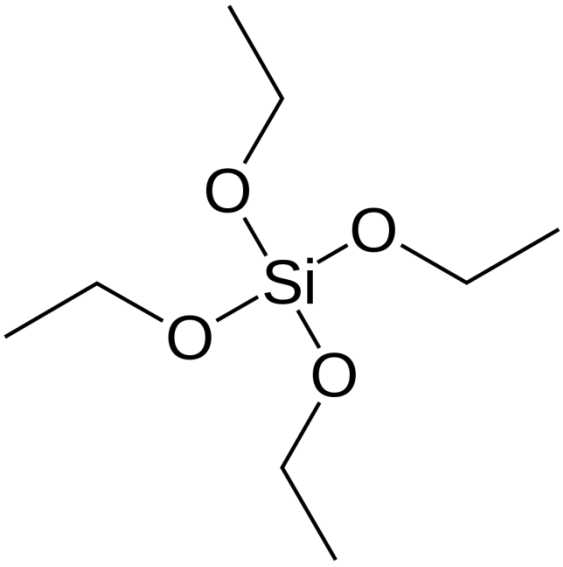

Figure 12. Tetraethyl orthosilicate (TEOS) [20]

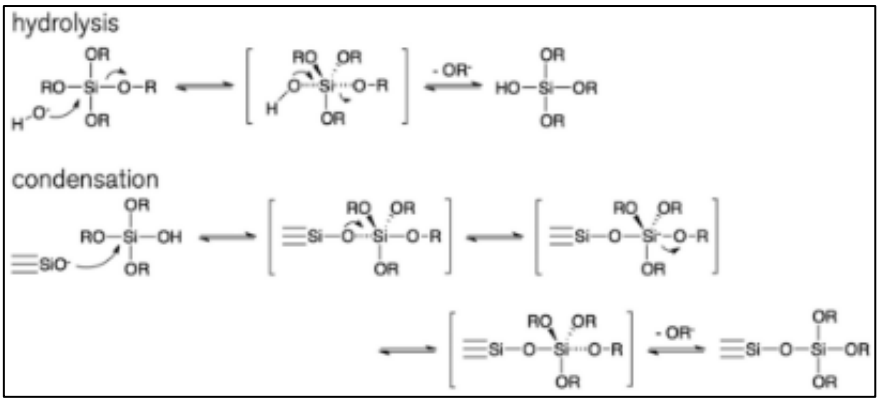

Figure 13. Base-catalyzed hydrolysis and condensation of TEOS [21]

The SiO_2 NPs were recovered through centrifugation at 10,000 rpm. The NPS were then washed with 2-methoxyethanol and again recovered through centrifugation. The washed NPs were finally dispersed in fresh 2-methoxyethanol. The concentration of SiO_2 NPs was measured by evaporation of a known volume of the solution and weighting the residue.

The synthesis of titanium sol gel, based on the hydrolysis of titanium alkoxides and its deposition as thin film on glass support, is a well-known procedure described in many articles [22],[23],[24],[25], and[26]. In order to synthetize the sol-gel, 38 mL of Titanium isopropoxide (TTIP, see Figure 14) was mixed with 206 mL of 2-methoxyethanol for one hour. A fraction of this solution was mixed with the solution containing the SiO_2 NPs in order to have a final volume of 80 mL and a composition of 80/20% in SiO_2/TiO_2. Different SiO_2/TiO_2 ratios have been tested by other collaborators of the project, and this ratio has been determined as being the one maximizing the SiO_2 percentage. In fact with a smaller concentration of TiO_2 gel, not enough adhesion is obtained. Just before the dip coating a solution containing 5.2 mL of deionized water in 206 mL of 2-methoxyethanol was added and stirred for 30 minutes in order to achieve the gel formation. The volume of the water solution added corresponds to the volume of the TiO_2 solution added in the silica-titanium mixture. In the same way than for the SiO_2 NPs, the titanium isopropoxide undergoes hydrolysis followed by condensation. This time, under non basic conditions, the result is not NPs but a TiO_2 gel matrix. Hydrolysis leads first to a dispersion of colloidal particles in a liquid (the so called sol) and further hydrolysis leads then to the more crosslinked gel [27]. To avoid a too fast reaction rate, and so the loss of homogeneity, and morphology and structure control, it is important to have a small concentration of water in the medium [27]. This explains the reason of the small water content in the water/2-methoxyethanol solution.

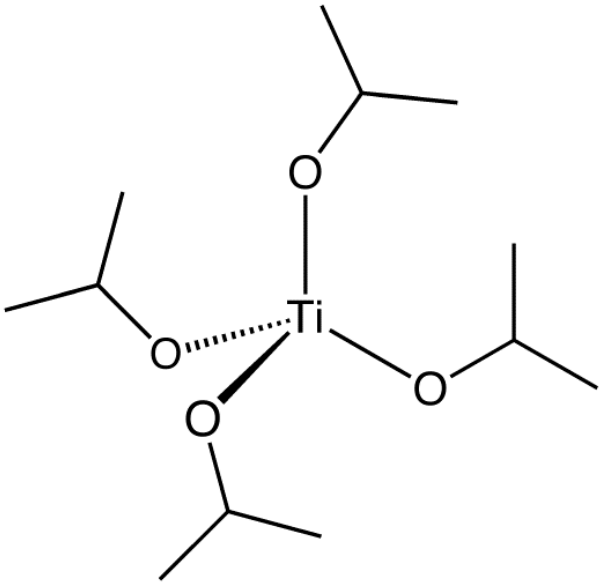

Figure 14. Titanium isopropoxide (TTIP) [28]

Before the dip coating, the glass slides had to be cleaned with a mixture of hydrogen peroxide and sulfuric acid, the "piranha solution". This mixture was done by adding 32 mL of a hydrogen peroxide (30 wt. %) solution into 90 mL of sulfuric acid (96 wt. %). The glass slides were dipped in this solution for one hour and then cleaned with deionized water. This method is a well-known method that removes impurities from the glass slides and hydroxylates the surface [29]. This helps to maximize the homogeneity of the coating onto the glass slides.

For the dip coating, the RDC 21-K Dip Coater, produced by Bungard-Elektronic Gmbh & Co., was used (Figure 15). The cleaned glass slides were dipped into the sol gel with a speed of 200 mm/min. They then stayed in the solution for 20 seconds before being pulled out again with a speed of 200 mm/min. The glass slides finally underwent a heat treatment in an oven at 150°C for one hour. The goal of this heat treatment was to achieve condensation between the titanium matrix (Ti-OH) and the hydroxyl groups on the glass surface (Si-OH) [23]. This operation was repeated 3 times in order to obtain 3 layers on the slides. Indeed the thickness of the film should be directly proportional to the number of times this operation is repeated [24]. The same operation was tested with a 60 mm/min dipping and pulling speeds in order to optimize the dip coating process.

Figure 15. RDC 21-K Dip Coater (Bungard-Elektronic Gmbh & Co. [30]

Finally RB is coupled with the SiO_2 NPs. The problem is that the synthetized SiO_2 NPs and the titanium coating have hydroxyl groups (-OH) at the surface and are thus negatively charged. Because RB in solution is negatively charged and does not have an electrophilic site they cannot react with the surface of the coating (composed of the TiO_2 matrix and the SiO_2) hydroxyl groups. Thus the surface of this coating has to be functionalized in order to change the charge at the surface. This is achieved with the help of an alkoxyorganosilane, in our case APTES (Figure 5), which presents an amino group on that RB can be attached [19]. To do so the coated slides are submerged during one night into a solution containing 1 mL of APTES in 50 mL of toluene. The glass slides are then washed with distilled water and dipped for one hour in 54 mL of a 1g/L water solution of RB together with 0.5g of the water-soluble EDC (Figure 6) as coupling agent. EDC allows specific conjugation between the amino group on the SiO_2 NPs and the carboxylic acid group of RB. It works by activating the carboxylic groups in order to facilitate the amide bond formation with an amine. The mechanism of coupling a carboxylic acid and RB is shown in Figure 16: First the EDC reacts with the carboxylic group of RB to form an O-acylisourea intermediate. This intermediate can then easily undergo a nucleophilic attack from the amino group of SiO_2 NPs to form an amide bond. The formed byproduct is a water soluble urea derivative [31]. The obtained glass slides have then a pink color (see Figure 17).

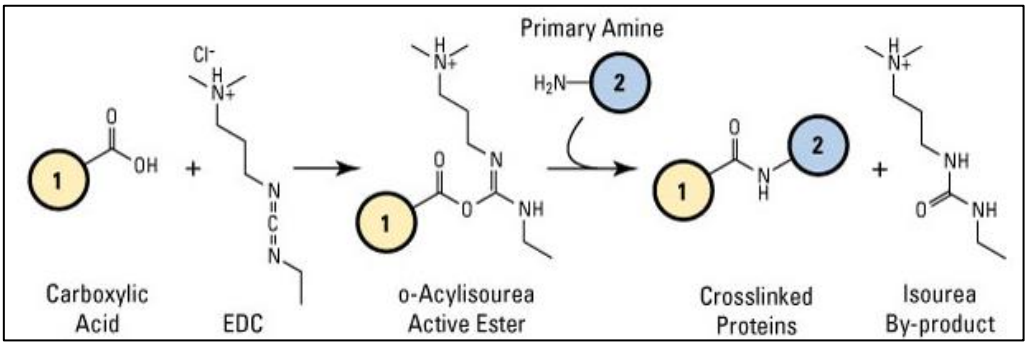

Figure 16. EDC coupling reaction scheme [31]

Figure 17. Functionalized glass slides

2.2 Mesoporous SiO_2-RB Nanoparticles

Like explained in section 5.1.4 RB coupled to dense SiO_2 NPs synthetized by the Stöber method degrades too fast. For this reason it has been tested to synthetize mesoporous SiO_2 NPs in order to attach at least a part of the RB inside of the pores. Indeed working with mesoporous SiO_2 NPs presents two main advantages: First of all, porous materials have a larger surface area and so allow a higher loading of RB. Secondly porous inorganic materials are known for protecting the loaded molecules, in our case RB, from photochemical degradation [32]. These two reasons gave us hope to significantly increase the lifetime of the loaded SiO_2 NPs by slowing down the bleaching process of RB. Additionally, mesoporous SiO_2 NPs have accessible adsorption sites in high concentration, undergo fast mass transfer, have an easily modifiable surface and present a good thermal resistance [33]. With these NPs, two coupling agents were tested: EDC and HATU. The NPs were synthetized drawing inspiration from *Planas et al.* [34].

5.81g (16.94 mmol) of cetyltrimethylammonium bromide (CTAB, Figure 18), 130 mL of deionized water, and 23 mL of Ethanol were mixed together for one minute. 250 µL of ammonia (NH_3 30 wt %) was then added and the solution was stirred at 50°C. After 30 minutes, 15 mL (67.2 mmol) of TEOS was added dropwise and the solution was stirred for 2 hours at 50°C. The NPs were then allowed to age for 24 hours at ambient temperature. The mechanism of the formation is shown in Figure 19: The template surfactant, CTAB, forms micelles in aqueous solutions. The TEOS is then hydrolyzed and condensed around these micelles to form the NPs.

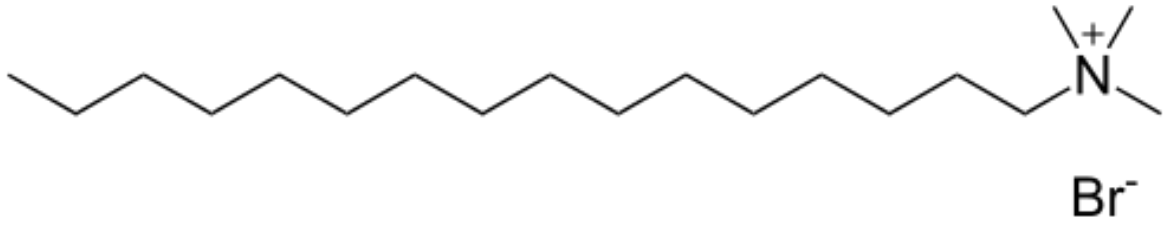

Figure 18. CTAB (cetyltrimethylammonium bromide) [35]

Figure 19. Templated mesoporous silica synthesis [33]

After allowing the particle to age, 40 mL of hydrochloric acid (HCl wt 37%) was added under agitation in order to remove the CTAB. The solution rested then for 12 hours in order to dissolve the entire template. The NPs were then recovered through centrifugation at 6000 rpm during 30 minutes. The mesoporous SiO_2 NPs were finally washed (dispersion in ultrasound followed by centrifugation) 3 times with ethanol.

The NPs were then dispersed in two times 50 mL of isopropanol and 1 mL of APTES was added in each solution. The surface modification was carried out during the night. The NPs were again recovered through centrifugation and washed one time with isopropanol and one time with ethanol.

The conjugation of the SiO_2 NPs with RB was tested with two different coupling agents. For the coating the procedure used was similar to the case of EDC: The NPs were dispersed in 100 mL water, and 100 mL of the 1g/L aqueous RB solution[1] together with 200 mg of EDC were added. The coupling reaction was carried out during 24 hours.

When working with HATU the conditions were slightly changed: First of all, the reaction with HATU has to be carried out in dimethylformamide (DMF). So the amino-functionalized SiO_2 NPs were dispersed in 100 mL of DMF instead of water. This solution was then mixed with 200 mL of a 1g/L ($1.9654*10^{-4}$ mol) RB solution[1] in DMF. To this solution, 0.075 g of HATU (1 equivalent) and 80µL of DIPEA (2.4 equivalents) are added to induce the coupling. Here again the coupling reaction was carried out during 24 hours. The mechanism of the coupling with HATU is shown in Figure 20: The first step is the deprotonation of the carboxylic acid function on the RB by the DIPEA followed by the attack of the resulting carboxylic anion on the electrophilic carbon of HATU to form the unstable *O*-

[1] The Rose Bengal used for the solutions in deionized water and DMF is the Rose Bengal disodium salt (MW = 1017,63 g/mol)

acyl(tetramethyl)isouronium salt. The anion of this formed salt then attacks the carboxylic acid derivate of its cation to form an active ester and liberates a stoichiometric quantity of tetramethylurea. Finally, the acylation takes place between the active ester and the nucleophile amine to form the amide bond [36], [37]. It is important to not add the HATU coupling agent in excess compared to the RB, because it can react with the amine and form a guanidinium by-product, which indeed lowers the efficiency of the coupling reaction [38].

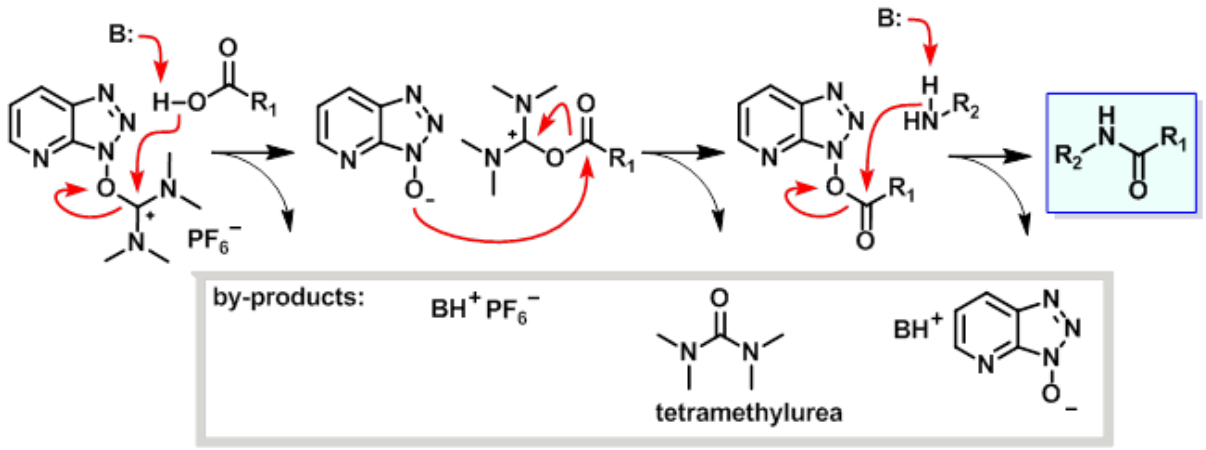

Figure 20. Coupling reaction between carboxylic acid and amine with HATU [37]

The NPs were recovered by centrifugation and washed (dispersion followed by centrifugation) in acetone to remove all the unreacted RB. This washing process was done until a clear and RB free solution is obtained after centrifugation. The SiO_2 NPs were then finally dispersed in water.

For these NPs, with the HATU coupling agent, a second functionalization has been conducted in order to couple a higher amount of RB to the SiO_2 NPs. The obtained differences are shown in the characterization part of this work.

2.3 Direct amino-functionalized SiO_2-RB Nanoparticles

This method, also known as the co-condensation method [33], was tested in order to have a more uniform repartition of the amino groups on the surface of the NPs and to avoid potential mass transfer problems of the APTES into the meso-pores. This method consists in adding simultaneously the TEOS and the APTES in order to condense both together. The NPs were synthetized by drawing inspiration from the following article [32].

3g of CTAB were dissolved in 250 mL of deionized water and heated to 80°C during 1 hour. 15 mL of TEOS and 2 mL of APTES were mixed together and added dropwise to the CTAB solution. This solution was heated at 80°C and stirred during 2 hours. The NPs were aged at room temperature during 24 hours and the template was then removed by adding 40 mL of HCl (37 wt%) and stirred during 12 hours. The NPs were recovered by centrifugation and washed with water and with ethanol. RB was finally coupled to the SiO_2 NPs with EDC following the same procedure than in section 2.2. For these NPs a second functionalization with EDC has been conducted to maximize the quantity of RB linked to SiO_2 NPs. The reaction conditions were the same for the 2 functionalization.

3. Characterization of the particles

3.1 Thermogravimetric (Tg) analysis

The thermogravimetric analysis of the SiO_2 NPs was performed in order to estimate the quantity of Rose Bengal (RB) attached to the SiO_2 NPs. This technique consists in heating up the material with a constant increase of temperature and measuring the mass loss of the sample. The fraction of mass of the sample remaining, compared to the initial mass, is plotted as a function of the temperature. The analysis was conducted between 400 and 800 °C. Analysis were done using the different NPs: Dense SiO_2 NPs, without RB and with RB coupled with EDC; Mesoporous SiO_2 NPs without RB, with RB and EDC as coupling agent, and one and two functionalization with HATU as coupling agent; and co-condensed SiO_2 NPs, without RB and with two successive coupling reactions with EDC. The thermal analyzer used for the measurements is the "SENSYS evo TG-DSC" from the French company "Setaram instrumentation" (Figure 21). The carrier gas used during the thermal analysis was air.

Figure 21. Thermogravimetric analyser [39]

The first analysis is the analysis of the dense NPs that have been used together with the TiO_2 matrix on the glass slides (see Figure 22). The analysis was conducted between 20 and 800 °C, the mass loss that occurs before 400°C was not taken into account because it has been attributed to water loss and non-attached RB.

It can be observed that the SiO_2 NPs weight lost is of 3.2% without RB and 10% with RB. It can by this way be deducted that the RB represents 6.8% of the weight of the NPs.

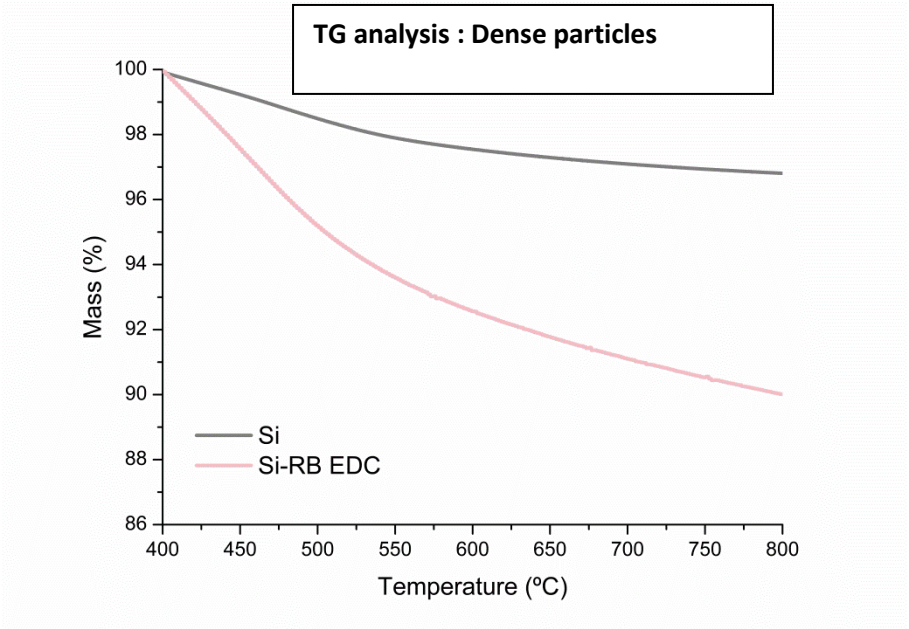

Figure 22. Thermogravimetric analysis of the dense silica nanoparticles

The second analysis concerns the mesoporous SiO_2 NPs (see Figure 23). Once again the thermogravimetric analysis is conducted between 400 and 800 °C and the mass loss before 400°C is not taken into account. Four curves are represented: the mesoporous NPs without RB (in black), the NPs with RB and EDC as coupling agent (in green), and the SiO_2 NPs with RB and HATU as coupling agent, after one functionalization (in red) and after two functionalization (in purple).

The weight loss of the mesoporous SiO_2 NPs without RB is of 4,5%, which is a little bit more than the weight loss of dense NPs. The weight loss of the NPs coupled to RB with EDC is of 11.6%, and so, when the weight loss of SiO_2 is taken into account, the RB corresponds to 7.1% of the weight of the NPs. When looking to the coupling with HATU, it can be observed that the first functionalization does not allow to reach as good results as with EDC: The weight loss is of 7,4% which corresponds to a RB loading of 2.9%. Only after the second functionalization a similar loading than with EDC could be obtained: 11.1 % weight loss, corresponding to a 6.6% mass fraction of RB for the NPs. The lower coupling with HATU can be explained by the fact that, in contrary to EDC, where the coupling agent is added in excess without having negative drawbacks, the HATU cannot be added in excess because of the undesired by-product formation [38].

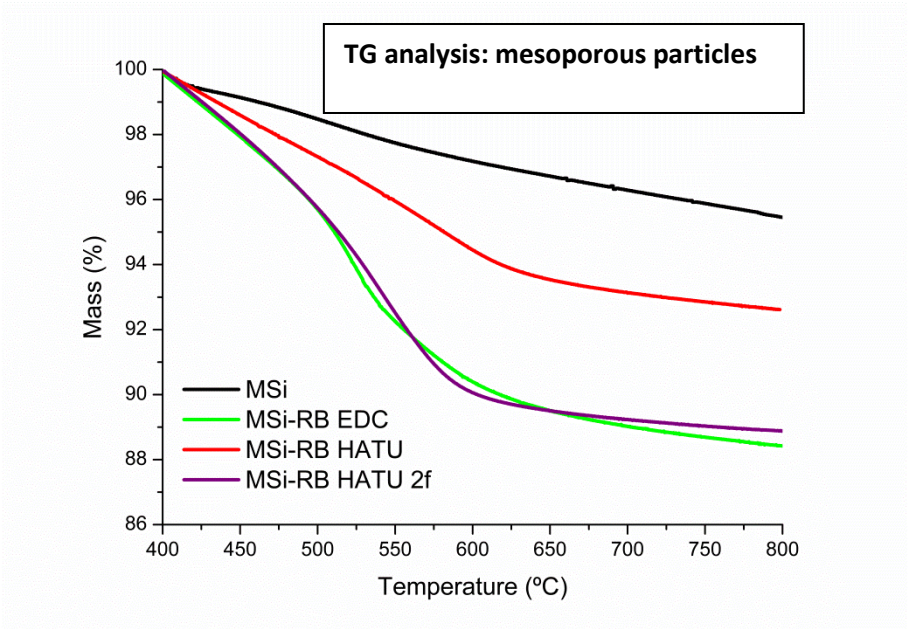

Figure 23. Thermogravimetric analysis of the mesoporous silica nanoparticles

The last analysis concerns the SiO_2 NPs obtained by co-condensation of the TEOS and of the APTES. These NPs will later, thanks to the BET isotherm analysis (section 3.3), be determined as being micro-porous NPs and will from this point be called as such. Like for the previous cases only the mass loss occurring after 400°C was taken into account and the analysis was conducted until 800°C. The results are shown in Figure 24. The blue curve represents the mass loss of the SiO_2 microporous NPs without RB while the orange curve represents the NPs after a two time functionalization with RB and EDC as coupling agent.

The first remark that can be made is that, compared to the dense and mesoporous SiO_2 NPs, the RB free microporous NPs have a much higher weight loss: 8,9% of weight loss between 400 and 800°C, which represents 4.4 % more than the mesoporous NPs and even 5.7% more than the dense NPs. These NPs seem to be more brittle and less thermo-resistant than the previous ones. Additionally it can be observed that the relative loading of RB on these NPs is relatively low compared to the other: The weight loss of the functionalized NPs is of 10,7 % which represents a loading of RB of only 1.8%. Finally it can be noticed that at the beginning of the Tg analysis, between 400 and 550 °C, there is a faster mass loss for the SiO_2 NPs without RB than the functionalized. This would mean that the NPs are stabilized, less brittle when the RB is attached in the pores and would lead to a better cohesion of the NPs at lower temperature. After 550°C the NPs do not lose SiO_2 anymore but the functionalized NPs continue to loose RB, leading to the fact that both curves cross again. Nevertheless the results seem strange because the NPs had an intense red color and the residual water in which the coupling was done was relatively clear and RB free after functionalization. The color effect could be explained by the fact that the micropores were too small to have mass transfer inside of the pores and so that all the RB was attached at the surface where it is particularly visible. Because of the evenly distributed amine groups due to the co-condensation, if functionalization only occurred at the surface, it would explain the low loading.

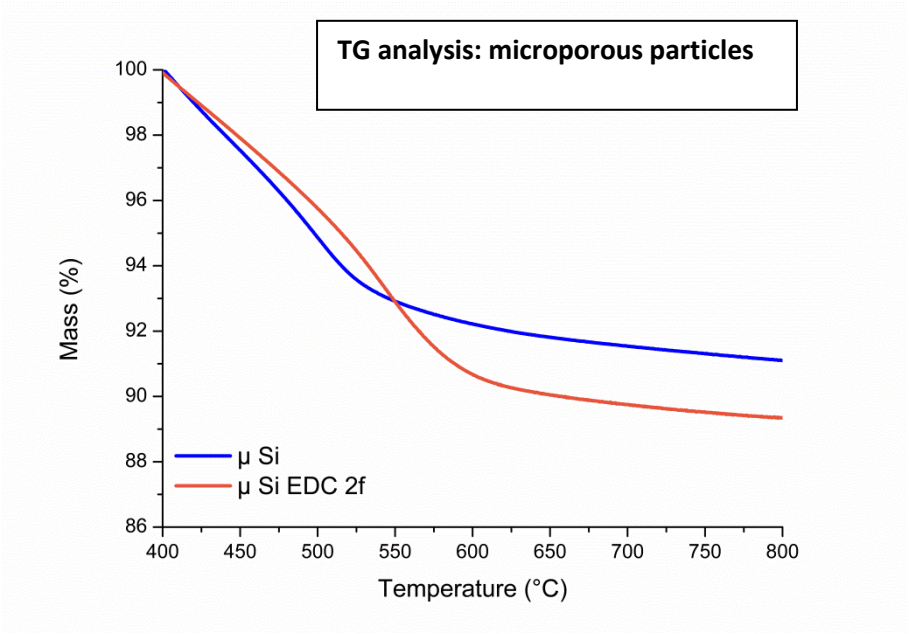

Figure 24. Thermogravimetric analysis of the co-condensed silica nanoparticles (microporous)

Table 1 and Figure 25 show a summary about the weight losses and the RB loading for all the different Nps. The mesoporous SiO_2 NPs coupled with RB either by EDC or HATU (2 times) show clearly the more promising results.

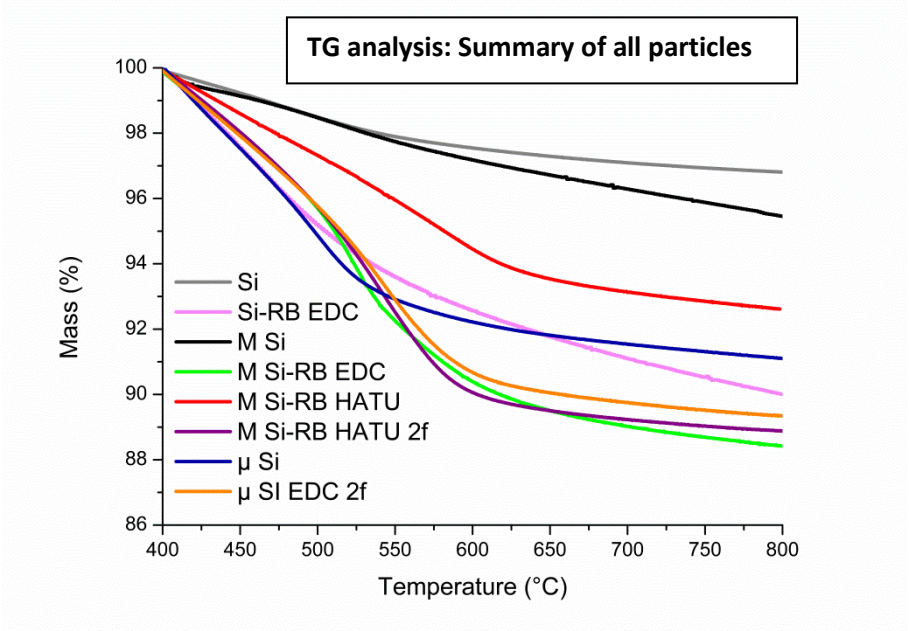

Figure 25. Summary of the Thermogravimetric analysis of all the particles synthetized and functionnalized

	Si	Si-RB EDC	M Si	M Si-RB EDC	M Si-RB HATU	M Si-RB HATU 2f	μ Si	μ Si EDC 2f
Mass loss (%)	3.2	10	4.5	11.6	7.4	11.1	8.9	10.7
% RB loading	-	6.8	-	7.1	2.9	6.6	-	1.8

Table 1: Summary of weight loss and Rose Bengal loading for the different silica nanoparticles

3.2 Profilometry

The profilometry analysis was performed on the glass slides used in the mesoreactor in order to measure the thickness of the film obtained after the dip coating. The measurements were made for dip coating speeds of 60 and 200 mm/min and in each case for one, two and three layers of film. The profile has been measured on each sample on a length of 200 µm. The profiles have been measured with the "Dektak 150 Surface Profiler" built by the U.S Company "Vecco" (Figure 26). The results are shown in Figure 27.

Figure 26. Profilometer [40]

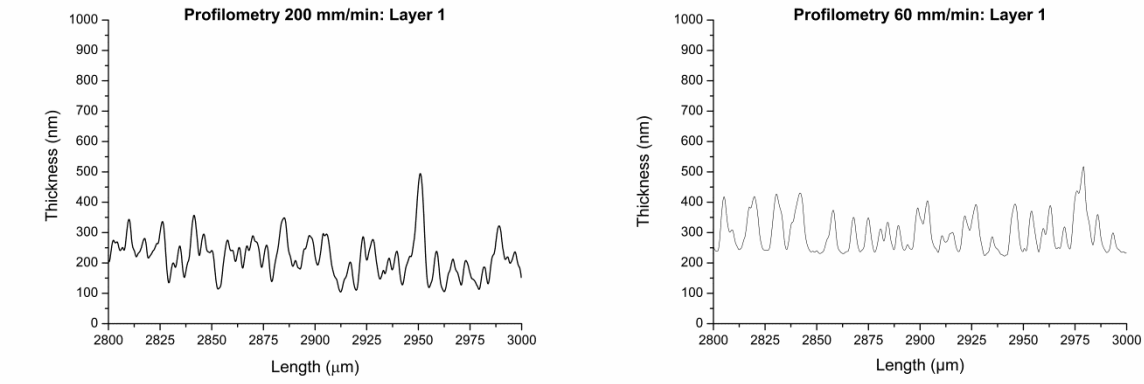

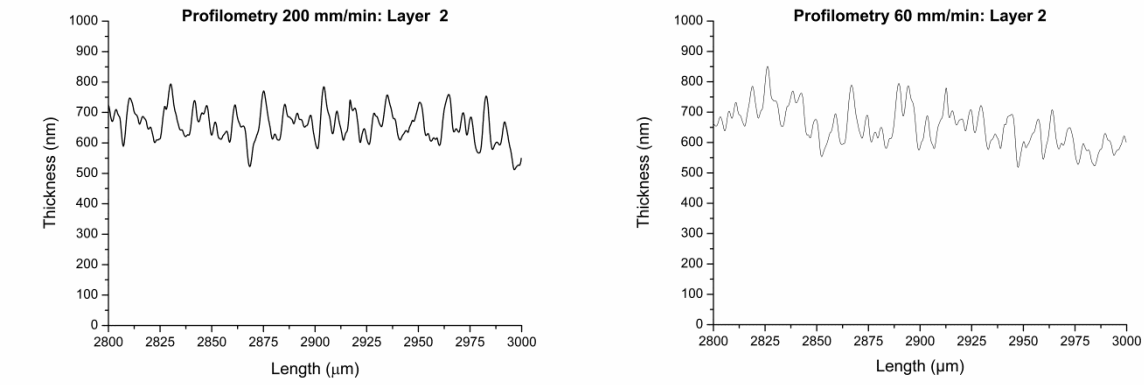

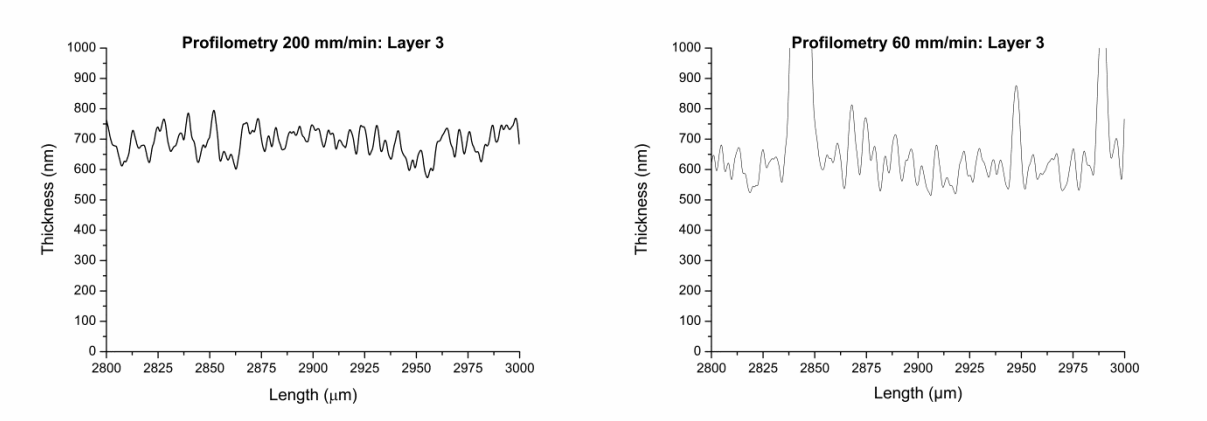

Figure 27. Profilometry of the dip coating glass slides for a dipping speed of 200 mm/min (right) and 600 mm/min (left) after 1, 2 or 3 layers

The first observation is that, in both cases, the thickness of the film increases between the first and the second layer: For the 200 mm/min speed the thickness after 1 layer is about 225 nm while after two dipping the thickness is around 650 nm. For the 60 mm/min the thickness of one layer is approximatively 325 nm, while after two layers the thickness is about 675 nm. The second observation is that the thickness does not increase significantly between the second and the third layer: There is a small increase, of the order of 25 nm, for the 200 mm/min speed while there is no observable thickness increase for the 60 mm/min speed but rather the irregularity of the coating increases. The last observation is that while the film thickness is more important after one layer for the 60 mm/min speed, the final thickness is equivalent with both methods after 3 layers. Also the roughness of both coatings has been measured: While the roughness of the fast dip coating is of 40, the roughness of the slower dipping only reaches 21. A higher roughness has the positive effect to offer more surface area and so more sites to attach the RB. This explains why later all the glass slides have been prepared with the 200 mm/min dip speed. This argument is supported by the fact that this method gives more regular coatings and the productivity reason, that allows to functionalize more glass slides in a given amount of time.

3.3 BET isotherms, BET Surface area, and BJH desorption Pore volume

The BET analysis have been done with the “ASAP 2420” surface area and porosity analyzer built by the Canadian company “Micrometrics” (Figure 28). By analyzing the BET isotherms it was possible to determine if the synthetized SiO_2 NPs are microporous, mesoporous, macroporous or non-porous materials. The BET surface area analysis gave us some information about the possible load in RB for the NPs. Finally, the BJH (Barrett, Joyner and Halenda) desorption method allowed us to obtain information about the pore volume. Before carrying out the measurements the samples underwent a heat treatment at 350 °C in vacuum during one hour in order to eliminate the moisture of the NPs.

Figure 28. N_2 adsorption-desorption equipment [41]

3.3.1 Dense nanoparticles

The first SiO_2 NPs that have been analyzed are the dense NPs synthetized by the Stöber method and used in the TiO_2 matrix coating. These NPs have been analyzed before and after coupling with RB by EDC. The results are shown in Figure 29.

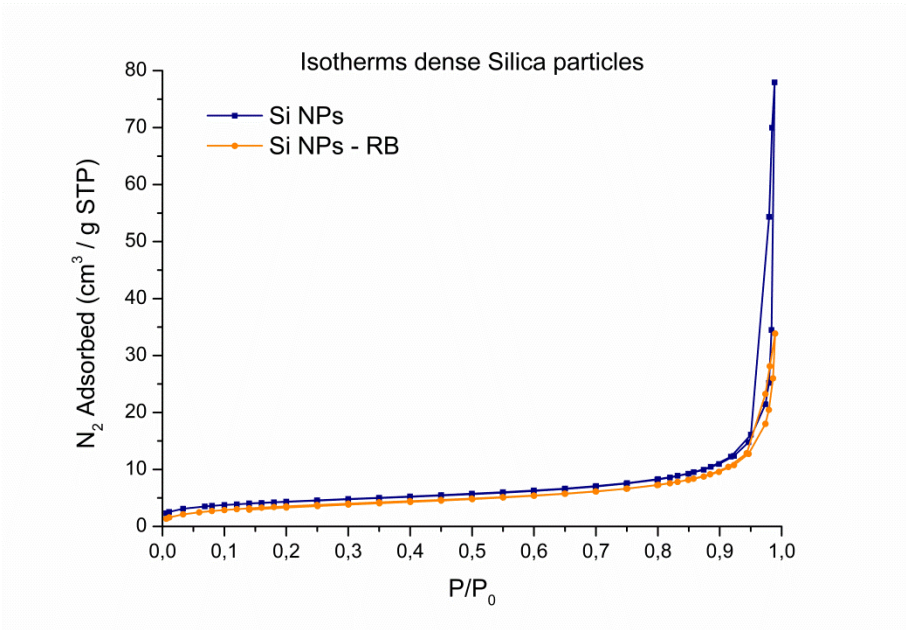

Figure 29. BET analysis: isotherms of dense SiO_2 NPs and dense SiO_2 NPs-RB functionalized with EDC

The isotherms clearly demonstrate that the NPs synthetized are dense NPs with few pores. The analysis gave a BET surface area of 15.16 m^2/g for the NPs without RB and a BET surface area of 13.07 m^2/g for the NPs coupled with RB. These are low values, and so again confirm that the NPs do not present significant porosity. The lower surface area can be explained by the fact that the few

pores present in the dense SiO_2 NPs are obstructed by coupled RB and so reduce the surface. Finally, the BJH desorption analysis provides information about the pore volumes (for pores between 1.7 and 300 nm diameter). The NPs with RB have a pore volume 0.0518 cm^3/g, while the NPs without RB have pore volumes of 0.1184 cm^3/g. This again means that the few pores that are present in the dense NPs are filled with RB.

3.3.2 Mesoporous nanoparticles

For the mesoporous SiO_2 NPs 4 BET measurements have been done: RB free mesoporous NPs, and the NPs coupled to RB with EDC or HATU. For the HATU, like in the Thermogravimetric analysis, the results after one functionalization and after a second functionalization are represented. The results are shown in Figure 30.

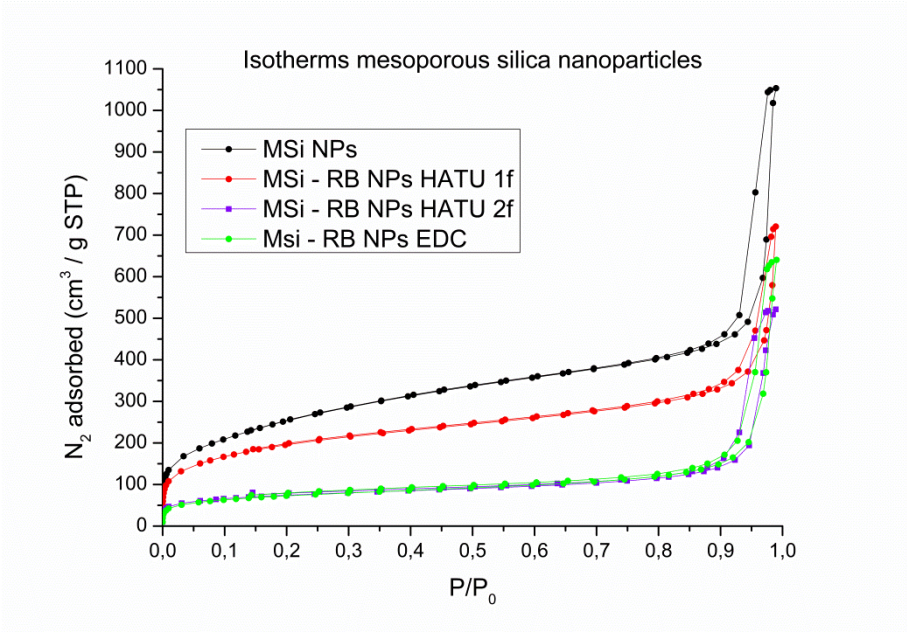

Figure 30. BET analysis: Isotherms of mesoporous SiO_2 NPs, and mesoporous SiO_2 NPs functionalized with EDC and HATU 1f/2f

In this case the isotherms obtained are typical for mesopores. It can be observed that the quantity of nitrogen adsorbed is much more important than in the case of the dense NPs. Also, the quantity of nitrogen adsorbed significantly decreases when the NPs are coupled to RB. This can be explained by the fact that the pores are filled with RB that decreases the specific surface and the volume of the pores. This theory is confirmed by the BET surface area measurements and the pore volume measurements. The BET surface area for the NPs without RB is of 926.63 m^2/g, while it decreases to 693.93 m^2/g after one functionalization with HATU and decreases further to 256.77 m^2/g after the second functionalization reaction. The surface area directly decreases to 255.97 m^2/g for the coupling done with EDC. The results in surface area are almost identical when NPs are functionalized two times with HATU or when they are functionalized with EDC. This can also been observed on the isotherms graph. Concerning the pore volumes, calculated with the BJH desorption method (taking into account pore having a diameter between 1.7 and 300 nm) the NPs without RB have a pore volume of 1.4933 cm^3/g. After one coupling reaction with HATU the pore sizes decrease to 0.9608 cm^3/g and decreases even further to 0.7391 cm^3/g after two functionalization reactions. When EDC is used as coupling agent, the pore volume decreases to 0.9315 cm^3/g. This last result

seems a little bit strange because the pore volume is higher than for two coupling reactions with HATU whereas the surface areas are the same and the RB loading also (see section 3.1). This could possibly be explained by the fact that the 3 dimensional attachment way of the RB inside the pores could be different when using EDC or HATU as coupling agent.

3.3.3 Microporous particles

The BET analysis has been done for the microporous SiO_2 NPs without RB, and after coupling reaction with EDC. Isotherms, surface area and pore volume have been measured before functionalization and after 1 or 2 functionalization reactions. Results are shown in Figure 31.

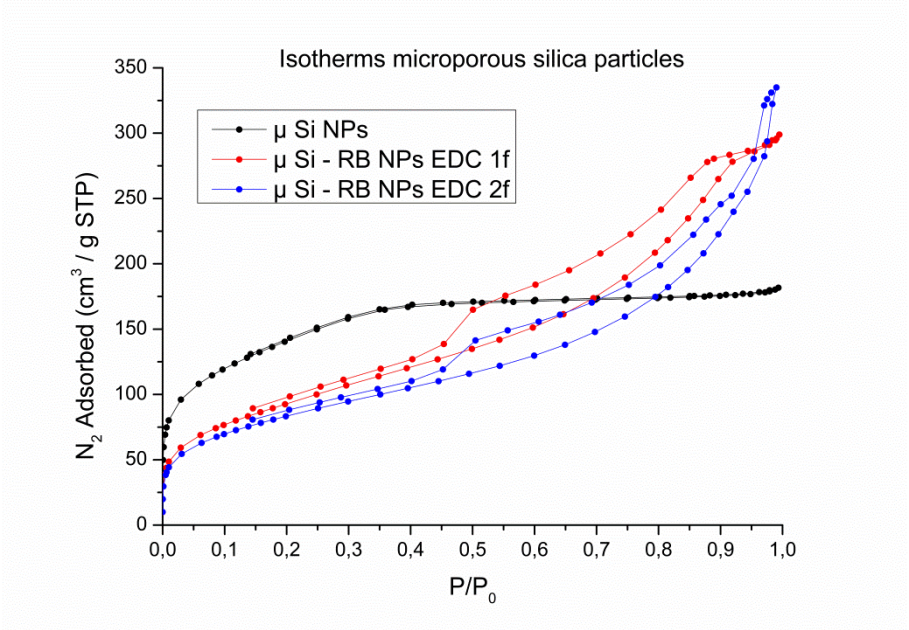

Figure 31. BET analysis: Isotherms of microporous SiO_2 NPs and microporous SiO_2 NPs functionalized with EDC 1 and 2 times

The results of this analysis are really interesting. Like already mentioned, in other sections, isotherms typical of microporous solids were obtained. Once the coupling reactions take place the structure seems to be changed and the NPs obtained have a mesoporous structure. At low relative pressure, less nitrogen is adsorbed with RB compared to the NPs without. This means that some of RB is attached into the micropores and so reduces their size. On the other side, at a little bit more elevated relative pressure, in the mesoporous range, the NPs continue to adsorb nitrogen and the 2 curves even cross each other. This means that at the end, more nitrogen is adsorbed and so that there is a higher pore volume. This could only be explained by the fact that RB attached at the surface of the NPs forms a new porous network, which in this case would be mesoporous. This hypothesis of forming a new porous network at the surface thanks to RB seems to be confirmed by the fact that the pore volume increases with each coupling reaction. The pore volumes (for pores with a diameter between 1.7 and 300 nm) measured with the BJH desorption method are 0.1620 cm^3/g before RB attachment, 0.4463 cm^3/g after the first reaction, and 0.4915 cm^3/g after the second reaction. Also the fact that mesoporous, or at least bigger pores, are formed is confirmed by the BET surface area measurements. The surface area decreases which each coupling reaction: Before RB attachment the BET surface was of 505.10 m^2/g and drops to 341.80 m^2/g after one

coupling reaction and to 303.39 m²/g after the second reaction. A higher pore volume with less surface area means of course bigger pores.

3.3.4 Summary

Figure 32 shows the isotherms of all the SiO_2 NPs obtained, before and after the coupling reactions. Table 2 summarizes the results obtained in terms of pore volumes and surface area.

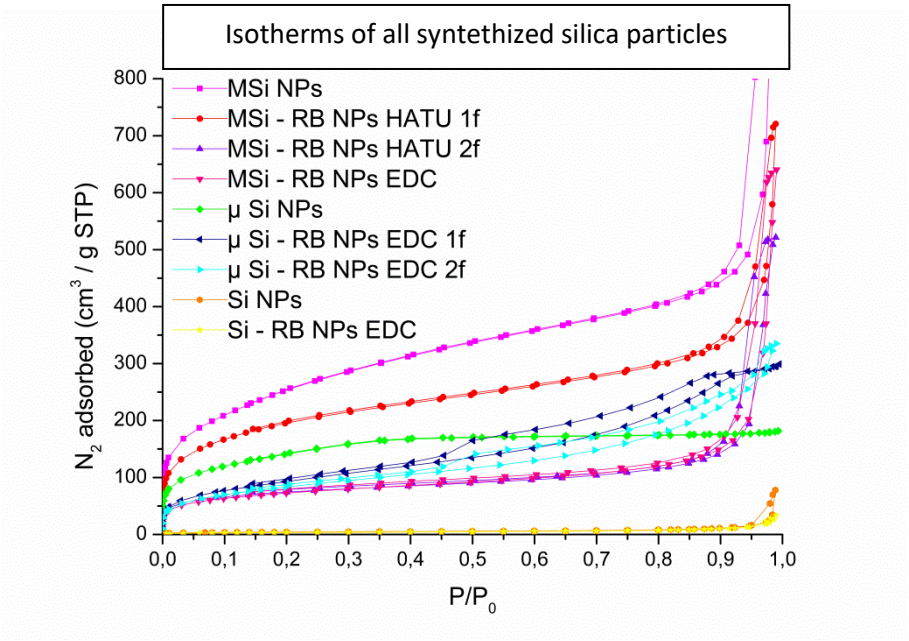

Figure 32. BET analysis: Isotherms of all the SiO_2 NPs synthetized and functionalized

Particle	BET Surface Area	BJH desorption volume of pores
Mesoporous SiO_2 NPs	926.63 m²/g	1.49 cm³/g
MSi NP + RB (EDC, 1f)	255.97 m²/g	0.93 cm³/g
MSi NP + RB (HATU, 1f)	693.93 m²/g	0.96 cm³/g
MSi NP + RB (HATU, 2f)	256.77 m²/g	0.74 cm³/g
microporous SiO_2 NPs	505.10 m²/g	0.16 cm³/g
µSi NP + RB (EDC, 1f)	341.80 m²/g	0.45 cm³/g
µSi NP + RB (EDC, 2f)	303.39 m²/g	0.49 cm³/g
Dense SiO_2 NPs	15.16 m²/g	0.12 cm³/g
Dense SiO_2 NPs + RB (EDC)	13.07 m²/g	0.05 cm³/g

Table 2: BET Surface areas and BJH desorption cumulative volume of pores for all the particles synthetized and tested

The first observation that can be made on the isotherms is that, for a same type of NPs, the amount of nitrogen adsorbed decreases the most for the mesoporous NPs. This means that these NPs are the most filled with RB. For the dense NPs in contrary almost no change was observed in the isotherms with or without RB. This is due to the fact that there are almost no pores present, so they cannot be filled. This means that RB is attached at the surface of the NPs where it is not protected and so probably undergoes rapidly bleaching. Finally, the microporous NPs adsorb a little bit less nitrogen in the microporous region, meaning that some RB enters the micropores, on the other hand

adsorbs more nitrogen was adsorbed in the mesoporous domain, meaning that a new porous system is created when the NPs undergo the coupling reaction with RB.

In the Table 2 it can also be observed that compared to the porous materials, the surface area and the pore volume of the dense NPs are much lower. This surface area and pore volume decreases after the coupling reaction with RB, meaning that the few pores present are nevertheless fulfilled. In the case of mesoporous NPs, they present a huge surface area and a high pore volume. This means that RB can be attached inside of the pores. The pore volume and surface area decreased after functionalization with RB, meaning that the majority is attached inside of the pores where it is protected from bleaching. Finally, the microporous material presents a surface area in between the mesoporous and the dense NPs. The pore volume is only 50% higher than for the dense NPs, but in contrary to the macropores present in the dense NPs, is composed of micropores. The pore volume is nevertheless 10 times smaller than for the mesopores. This means that it is not possible to attach a high concentration of RB into the pores. Results show that some is attached into the pores, but also that a lot must be attached on the surface, where it creates a new mesoporous network. The mesoporous network can first of all be observed on the isotherm, but also by the fact that the cumulative pore volume increases while the surface area decreases, meaning an enlargement of pores.

After observation of all these results, the mesoporous SiO_2 NPs, and to a lesser extend the microporous NPs, seem clearly as being the most promising for the $^1O_2$ production. The majority of the work done in the microreactor has thus been done with these mesoporous SiO_2 NPs.

3.4 UV-visible spectrum

The absorbance in function of the wavelength, between 460 and 700 nm, has been analyzed for the SiO_2 NPs that represent the main interest, meaning the mesoporous NPs. The NPs coupled with RB through both EDC and HATU have been analyzed. In addition the absorption spectrum of free RB has been added. These analyses have been done using a “GENESYS 10S UV-Vis” spectrophotometer built by the American company “Thermo Fischer Scientific” (see Figure 33). The obtained results are represented in Figure 34.

The first thing that can be observed is that the maximum absorbance peak is shifted a little bit in direction of the red light for the mesoporous NPs. This is in fact good news: In means that the RB is in a new electronical configuration due to a new environment. It is therefore a proof, or at least a good indication, that the RB is chemically linked to the SiO_2 NPs and not just physically adsorbed. It can also be observed that the maximum peak is not at the same wavelength when the coupling reaction has been done with EDC or HATU. Its maximum peak is at 553 nm for the HATU and at 563 nm for the EDC. For the free RB the maximum peak is at 550 nm. Also the extinction coefficient is different. At same concentration of RB (calculated with the Tg) the absorbance is much lower for the EDC. Because in both reaction, the coupling agent is not involved in the final formed material, both NPs, conjugated through EDC or HATU should be identical materials and so have identical absorbance. The only reason that could explain this phenomenon has already been mentioned in section 3.3.2: That the 3 dimensional arrangement of the attached RB inside of the pores is different when using different coupling agents. This would lead to a different electronic environment and so a different absorbance for both kinds of NPs.

Figure 33. GENESYS 10S UV-Vis (Thermo Fischer Scientific) [42]

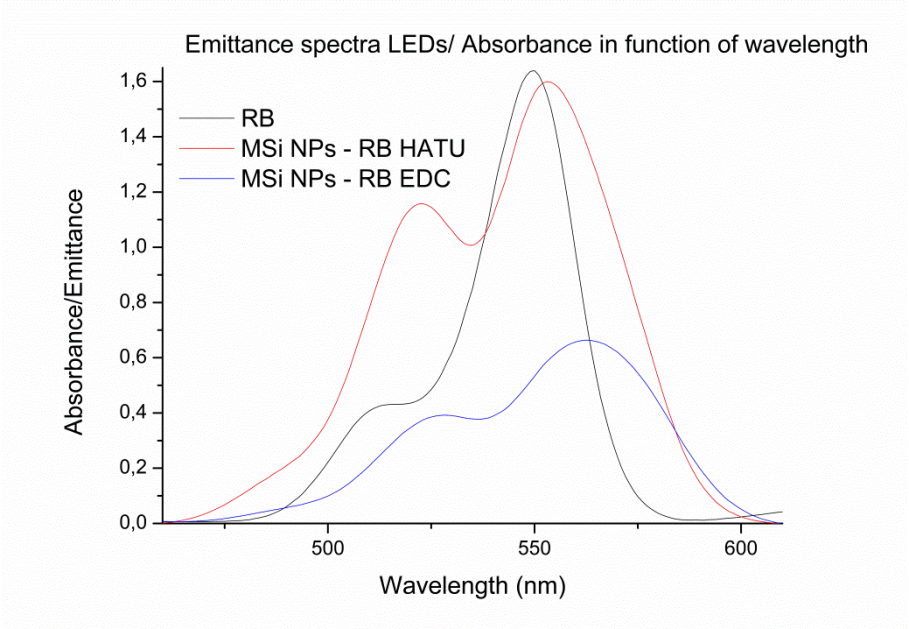

Figure 34. Absorbance of free Rose Bengal and Rose Bengal coupled through HATU or EDC to mesoporous nanoparticles. Measurements made in water.

4. Mesoreactor and Microreactor

In the following section, both used reactors are going to be described in addition to the light source characterization and the solvent choice justification.

4.1 Mesoreactor

This reactor has been designed and created for previous works [43].

As already mentioned in the introduction, this reactor cannot be considered as microreactor anymore because the lateral dimensions exceed 1 mm. In the other hand, its internal volume is of 2.4 ml, which is too small to consider it as a mesoreactor. It is in fact borderline between a mesoreactor and a microreactor. To ease the differentiation between both reactors it will nevertheless be called the “mesoreactor”. The reactive medium flows between two parallel glass slides which are irradiated with green light provided by LEDs (section 4.3). One of the two glass slides is coated with the TiO_2-SiO_2 matrix, functionalized with RB, obtained like explained in section 2.1.

The reactor itself is composed of 7 different rectangular layers composed of a hole in the middle to allow the inclusion of the 2 glass slides and the irradiation of the reaction medium inside of the reactor (Figure 35 and Figure 36). The two outer layers (a and g) have the dimensions of 120*60*5 mm and are made out of aluminum. The rectangular and centered hole has the dimension of 60*20*5 mm. The next layer (b and f) has the dimensions of 120*60*1 mm and is composed of white pigmented PFA. The hole in the middle has the dimensions of 60*20*1 mm. Layer c and e are also made out of white pigmented PFA and have as function to hold the two glass slides. Their dimensions are 120*60*1 mm while their holes have the dimension of 76.2*25.4*1 mm, which is exactly the dimension of the glass slides. Finally the layer in the center (d) is the layer where the liquid flows. It is once again made of white pigmented PFA and has the dimensions of 120*60*2 mm. Its centered hole, which determines the volume of the reactor, is of 60*20*2 mm. This leads to a volume of 2.4 mL. Layer a, b, and c have also two small holes at their extremities to allow the connection of the entering and leaving fluxes. Layer d has two small channels that connect the holes at the extremities of the layer to the main reactor part in the center. Their volume is not taking into account for calculating the reactors volume, because they are negligible compared to the rest of the volume. The entire reactor holds together by bolting.

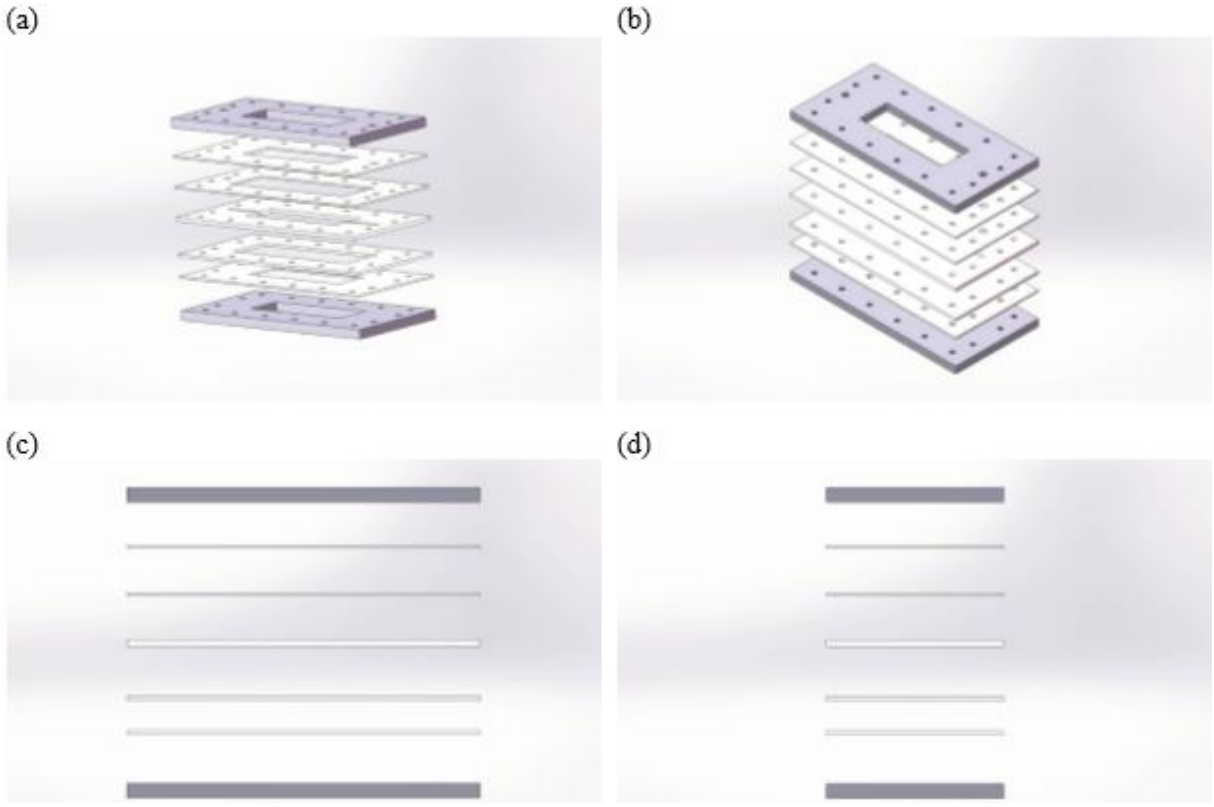

Figure 35. Assembly of the mesoreactor [43]

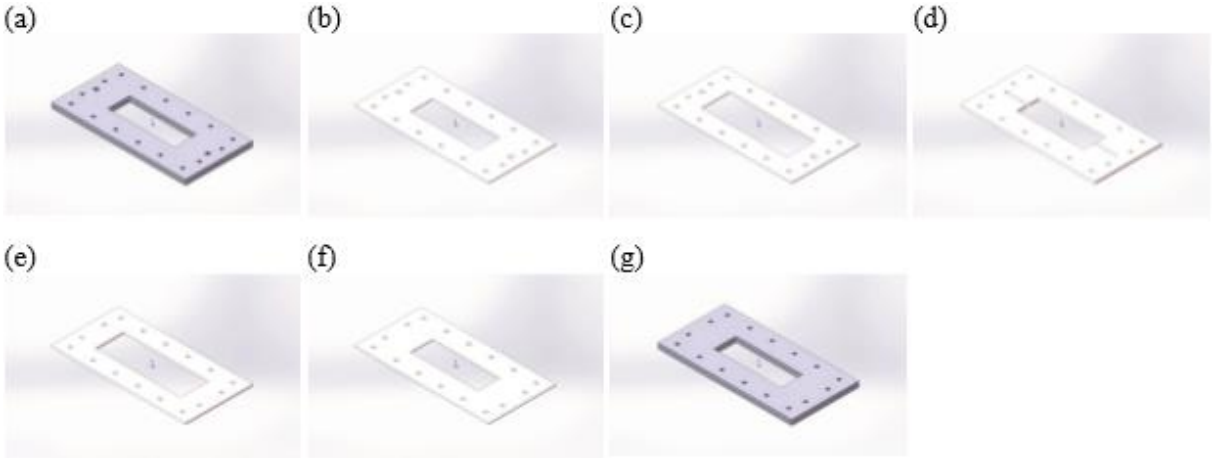

Figure 36. Representation of the different layers of the mesoreactor [43]

In order to inject the aqueous Met solution the "20 mL stainless steel syringe" manufactured by the American company Chemyx® was used. The "Nexus 6000 High Pressure Syringe Pump" from the American company Chemyx® (Figure 37) injected the liquid in the system, in order to deliver an automatic, precise and constant volume all along the process. To control the gas flow in the reactor, the "Gas Module" from the Dutch company Future Chemistry was used (Figure 38). Finally, the PFA tubing that connect all the different parts of the reactor as well as the connectors, like for example the "T" that mixes liquid and gas before injecting in the reactor come from the American company "Swagelok". The tubing used had an outside diameter of 1/8 of inch and an inner dimeter of 800 µm.

Figure 37. Nexus 6000 High Pressure Syringe Pump (Chemyx) [44]

Figure 38. Gas Module (Future Chemistry) [45]

This reactor was run under atmospheric pressure because, even after the use of good screws for the bolting and the use of silicone, some leaks resulted in liquid and gas flowing out of the reactor. These leaks were in particular out of control when working under pressure. The use of silicone also sometimes partially obstructed the channels of the mesoreactor, resulting in pressure spots and the breaking of one of our glass slides during one experiment.

The reactor was irradiated using 4 towers of green LEDs that are characterized in section 4.3. The reaction medium was water, and its choice is justified in section 4.4.

4 different experiments were done with this mesoreactor. Conversions were measured by NMR. The results are available in chapter 5:

Test 1: 1.49 g of Methionine was dissolved in 100 mL of water in order to have a 0.1M concentration solution. The gas used in this experiment was air. The liquid inlet flowrate was of 0.5 mL/min and the gas inlet flowrate was 1 mL/min. The current intensity of the LEDs was of 0.72A. Lams were disposed all around the reactor with a 90° angle to each other and formed so an "X shape". Samples were collected every 12 minutes.

Test 2: This test was done in the same conditions than the previous one (same concentration, gas and liquid flowrate, current intensity) but the lamps were disposed parallel to each other and perpendicular to the reactor window.

Test 3: The same concentration of Methionine (1.49g in 100 ml; 0.1M) was used with the same inlet flowrate (0.5 mL/min). The gas used was again air, but this time the flow rate was of 20 mL/min. The current intensity was again the same and the lamps were disposed, like in test 2, perpendicular to the reactor windows.

Test 4: The conditions were the same than in test 3 (0.1 M methionine with 0.5mL/min flowrate; gas at 20 mL/min flowrate; 0.72A current intensity), except that the nature of the gas has changed: Instead of air, this time pure O_2 was used.

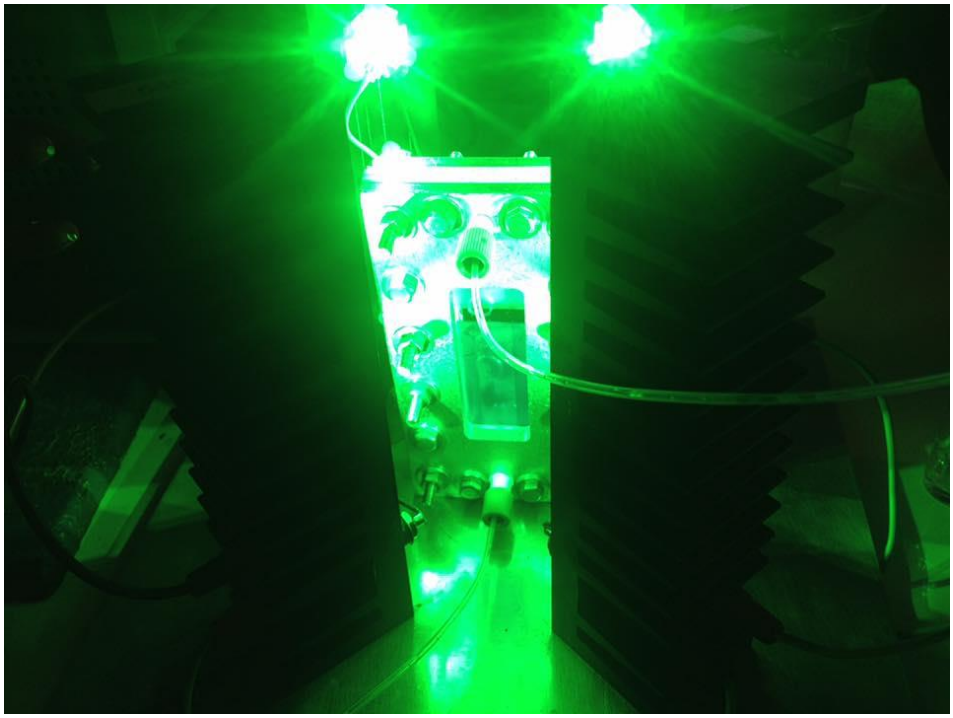

Figure 39. Mesoreactor in the "X" configuration (test 1)

Figure 39 shows the reactor running during the Test 1, with the lamps in the "X" configuration. The inlet flow is connected at the bottom of the reactor while the outlet is at the top. This allows the gas bubbles to pass through all the liquid and gives thus a better mixing and a better mass transfer of the gas into the liquid.

4.2 Microreactor

This reactor was composed of a PFA tubing (1/8 of inch outer diameter; 800 µm inner diameter) wrapped around a glass cylinder of 5 cm diameter. In the inside of the cylinder 60 LEDs

were glued in order to illuminate the reactor from the inside. To illuminate the outside, the 4 LED towers used for the mesoreactor were positioned around the glass cylinder with a 90° angle to each other in order to form a "X" shape and have the most homogeneous light distribution. As for the mesoreactor, the "20 mL stainless steel syringe" and the "Nexus 6000 High Pressure Syringe Pump" from Chemyx (Figure 37) are used to inject the liquid inside of the reactor. Also, the gas flowrate was controlled by Future Chemistry's Gas module (Figure 38). The PFA tubing that connect all the different parts of the reactor as well as the connectors still come from the American company "Swagelok". In contrary to the mesoreactor we were able to work under pressure. To keep a constant pressure inside of the reactor, a back-pressure regulator (Figure 40) from the American company "Zaiput Flow Technologies" was used.

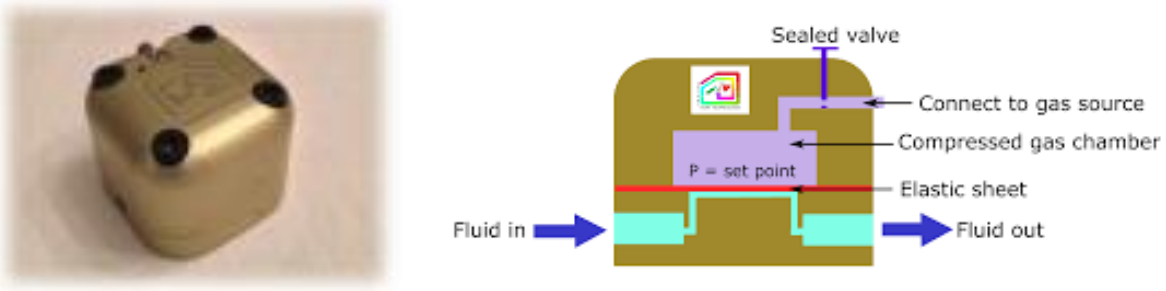

Figure 40. Back pressure controller [46], [47]

Two tubing lengths were tested during the experiments: A 2 meters reactor, leading to an interior volume of 1 ml, and a 4 meters reactor leading to an interior volume of 2 mL. The LED's used to irradiate the medium are the same than in the mesoreactor and are characterized in section 4.3. The reaction medium was still water (justified in section 4.4). Conversions for all the experiments have been measured by RMN and they are available in the "results" section.

For this reactor only one family of particles has been tested: mesoporous SiO_2 NPs. Indeed, the dense NPs did not show promising results neither with the TG analysis nor with the BET analysis. In addition, the mesoreactor showed that the RB attached to dense NPs, used in the glass slides coating, underwent a fast bleaching. The microporous particles were planned to be tested but they segregated too fast in solution, either because of a too high density or because of agglomeration. It was thus impossible to inject a homogeneous solution in the reactor and so to make some relevant tests.

Different series of test have been done, where all of the different parameters (length of reactor, liquid flow rate, pressure and concentration of RB particles) except one were kept constant. The concentration of methionine was in each case of 0.1M. The gas used was in each test pure oxygen with a flow rate of 15 mL/min. Concentration of RB in solution was determined knowing the amount of NPs dispersed in the aqueous Met solution and their RB loading was calculated with the help of the Thermogravimetric analysis. It could so be possible to calculate a "concentration" of RB in solution.

Series 1 - Variation of the reactor's length: The back pressure of the reactor was set to 6.9 bar. The concentration of RB was fixed at 0.45 mM. The liquid flow rate was 0.5 mL/min. The two tested reactor lengths were of 2 and 4meter.

Series 2 – Variation of the Rose Bengal concentration: The back pressure was still of 6.9 bar. The 4 meter reactor was chosen. Liquid flow rate was 0.5 mL/min. The different RB concentrations tested were of 0.45, 0.9 and 1.35 mM.

Series 3 – Variation of the liquid flowrate: The back pressure was set to 6.9 bar. The reaction was again carried out in the 4 meter reactor. The chosen RB concentration was of 0.45 mM. The 3 tested liquid flow rates were of 0.25, 0.5 and 0.75 mL/min.

Series 4 – Variation of the pressure: This last series of experiments was again completed in the 4 meter reactor, with the 0.45 mM RB concentration and the 0.5 mL/min liquid flowrate. The two tested pressures were 6.9 and 8.5 bar.

These 4 series were done with mesoporous NPs coupled with RB by EDC. To compare the EDC and HATU coupling agent, NPs coupled with RB by HATU were employed, repeating all these series but fixing the length of the reactor at 4m (series 1 is not repeated).

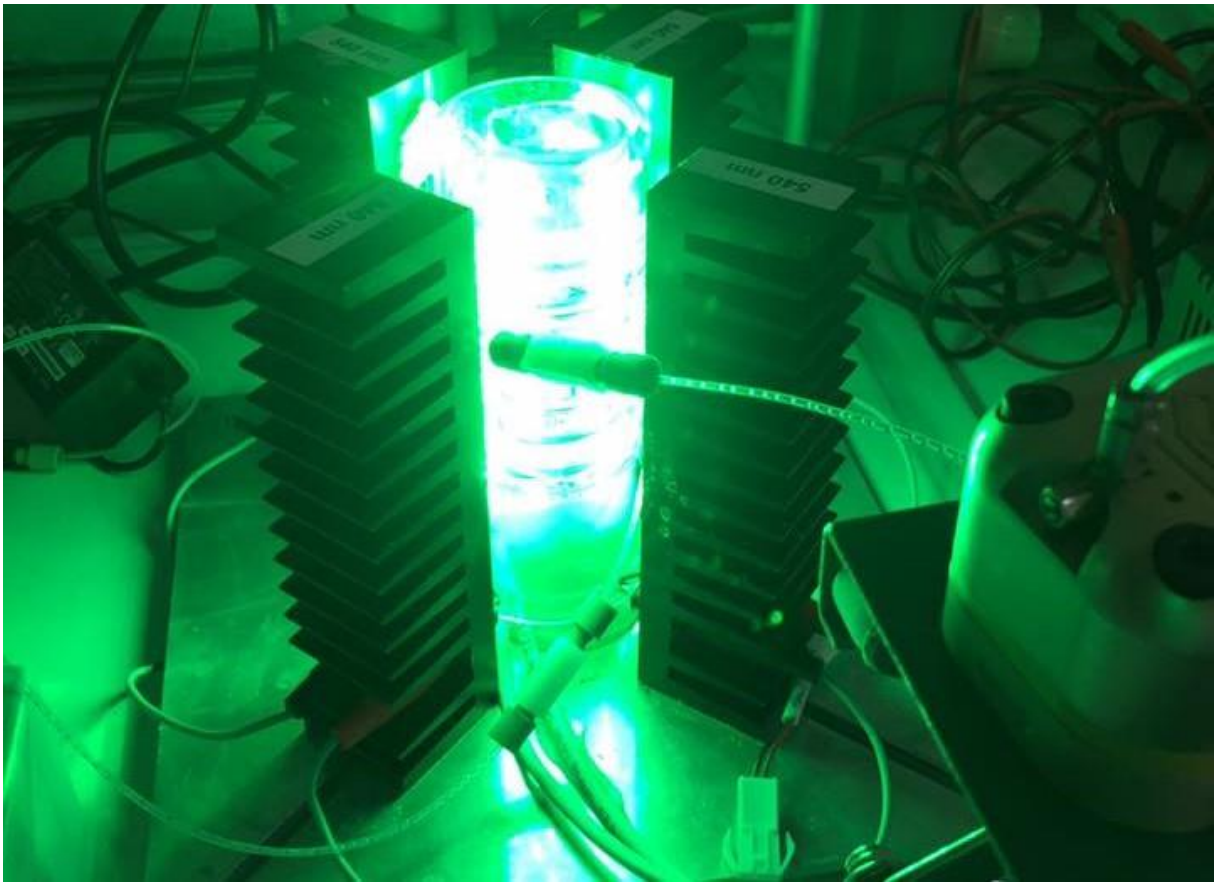

Figure 41. Microreactor

Figure 41 shows the microreactor while operating: The liquid-gas biphasic mixture enters the reactor at the bottom and leaves it at the top before entering into the back pressure controller that fixes the pressure in the entire reactor. Figure 9 shows the reactor in itself with the segmented flow.

4.3 Light source characterization

The light source is an important choice when studying photochemical reactions. It is important to have the greatest overlap between the light spectrum emitted and the absorption

spectrum of the catalyst, in our case the RB photosensitizer. Free RB in solution has its maximum adsorption at 550 nm wavelength [11]. RB coupled to SiO_2 NPs has an adsorption that is maximized at 563 nm when it is coupled by EDC and at 553 nm when the coupling agent is HATU (see section 3.4). All these wavelengths correspond to the green light of the light spectrum. So 2 choices are available for the light source: Either a halogen lamp can be used, that emits light in the entire visible light spectrum, which means a broad wavelength distribution, or the use of specific green light LEDs that have a significantly tighter wavelength distribution. This work focused mainly on the second option mainly due to the tight wavelength distribution that avoids activation of other molecules in the system leading to undesired byproducts through unappropriated light energy. Other advantages of LEDs are their low price, their energy efficiency [11], and the fact that, in contrary to the halogen lamp, they don't need an external cooler.

Figure 42 represents the luminous emittance of the green LEDs as a function of the voltage that is applied. To have a current intensity of 0.72 A, a voltage of approximatively 21 V was applied. This means that more or less 100 000 lm/m² were emitted. Figure 43 shows the wavelength distribution of the light emitted by the green LEDs. Its maximum peak is at 556-557 nm and so is closer to the particles functionalized with HATU than the particles functionalized with EDC.

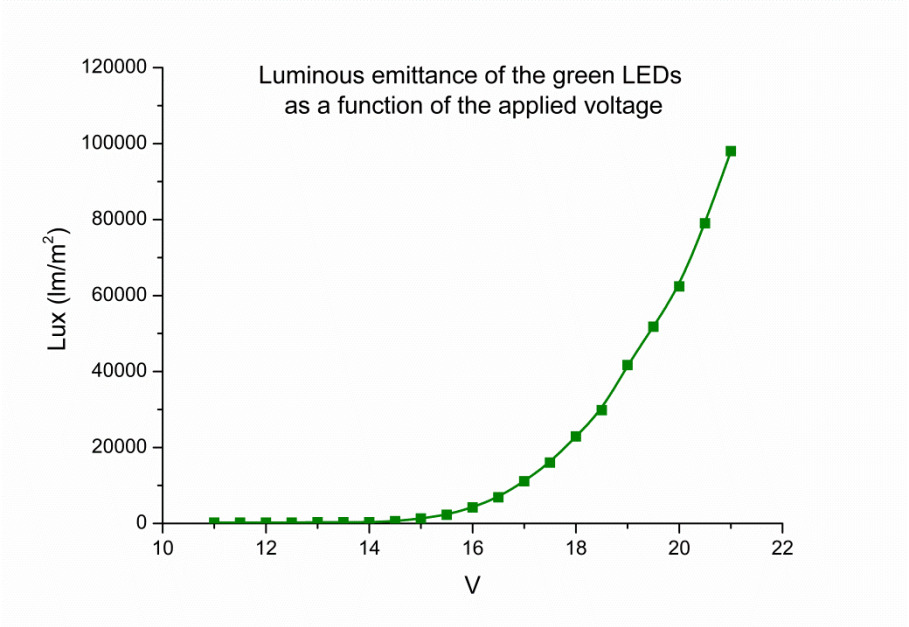

Figure 42. Illuminance of the green LEDs

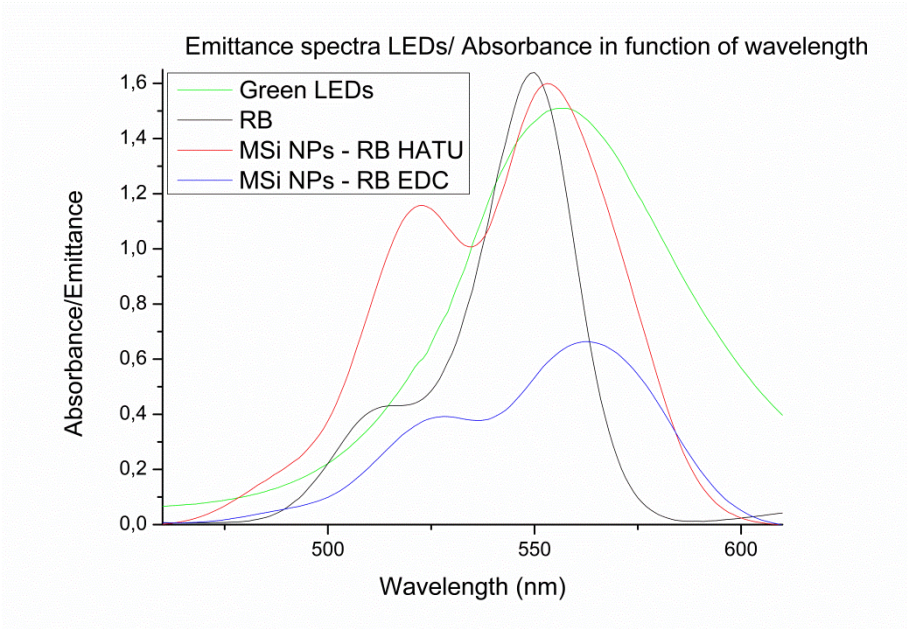

Figure 43. Emittance spectra of the green LED's and Absorbance spectra of RB and the NPs

4.4 Solvent choice

First of all, using water as solvent allows us to practice "green chemistry". It is in fact a cheap, environmental friendly and the most common solvent.

In addition to the "sustainability" point of view, the solubility of Met in water is relatively acceptable: 56.6 g/L at 25°C (0.38M) [48]. Especially compared to other common solvents like acetic acid (slightly soluble), and absolute alcohol, (petroleum) ether, benzene and acetone (all insoluble) choosing water makes common sense [49]. The oxidized form, MetO, is also soluble in water, namely up to 54 g/L [50].

The use of water as solvent is also a good choice because it is almost transparent to the visible spectra and so also to green light: The absorbance coefficient of pure water varies between 0.0474 and 0.0619 m^{-1} in the 540 the 560 nm range [51] (Figure 44). It can be observed that the light absorption for water is really low for blue light and still low for green light. Light absorption when using water becomes only problematic when using (infra)red light.

In addition to the solubility and the light absorption, using water has also another advantage: Its density is often higher compared to other solvents. While water, at temperature of 20°C, has a volumetric mass density of 0.998 kg/L, ethanol (0.789 kg/L), acetone (0.7845 kg/L), benzene (0.8765 kg/L) and petroleum ether (0.656 kg/L) have a lower density at the sale temperature. Acetic acid in contrast has only a slightly higher density (1.0446 kg/L) at 20 °C [52]. This allows the SiO_2 NPs to have a more important buoyancy force, and so to segregate more slowly. This results in more homogeneous solutions.

The drawback of $^1O_2$ is that its lifetime is highly solvent dependent and unfortunately is really short in the case of water: Between 3.1 and 4.2 µs (results vary depending on the method used to test its lifetime), while its lifetime in solvent like acetone (25-65 µs), Benzene (14-35 µs), Ethanol (9.6-16 µs) are approximatively of one order of magnitude longer. It is even possible to gain 2 or 3 orders

of magnitude in most of the chlorinated solvents, going even up to 4 orders of magnitudes (25-30 ms) for carbon tetrachloride, the solvent that allows the longest lifetime for $^1O_2$ [6].

The quantum yield of Rose Bengal in water at pH 7 is of 0.76, which is slightly lower than in methanol (0.8). The maximum quantum yield for Rose Bengal is obtained in benzylalcohol (0.95) [53].

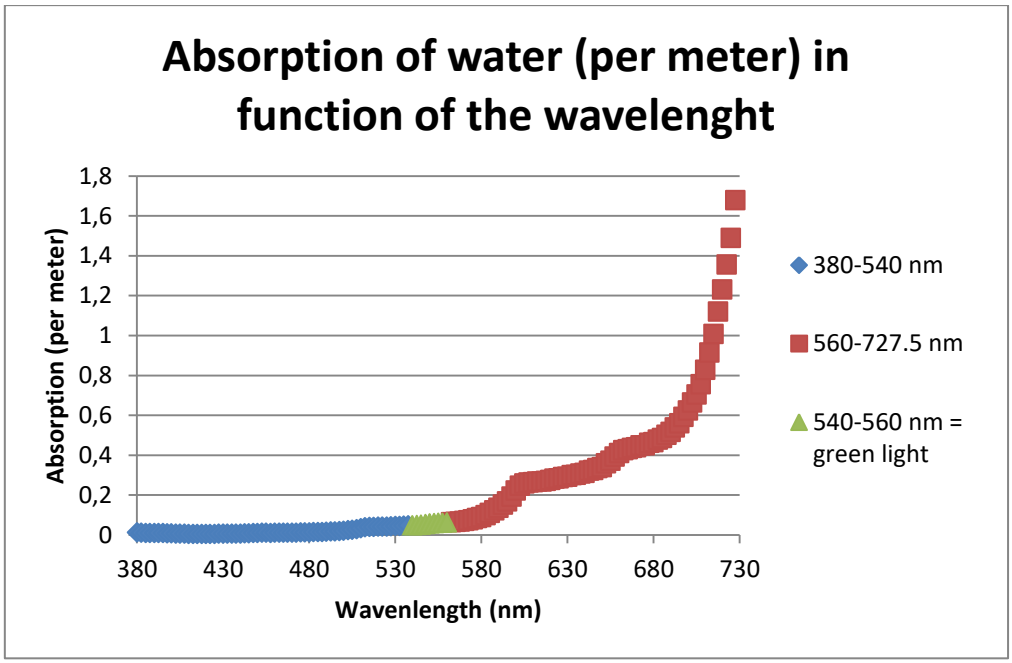

Figure 44. Water absorption in function of the wavelength. Data coming from [51]

5. Results

5.1 Mesoreactor

5.1.1 Test 1

The results of this first experiment are depicted in Figure 45. In contrary to the 3 other tests, the LEDs are positioned in a “X shape”, with a 90 angle to each other around the reactor. The reactor windows are illuminated with a 45° angle. It can be seen that the concentration of Met decreases during a long time and then stabilizes only after more than 100 minutes, almost 2 hours. It means that it takes a certain time, once the reactor is started, to reach steady-state. After almost 2 hours of running the results become more or less constant, with a resulting % of Met around 91.5% and so a conversion of 8.5%.

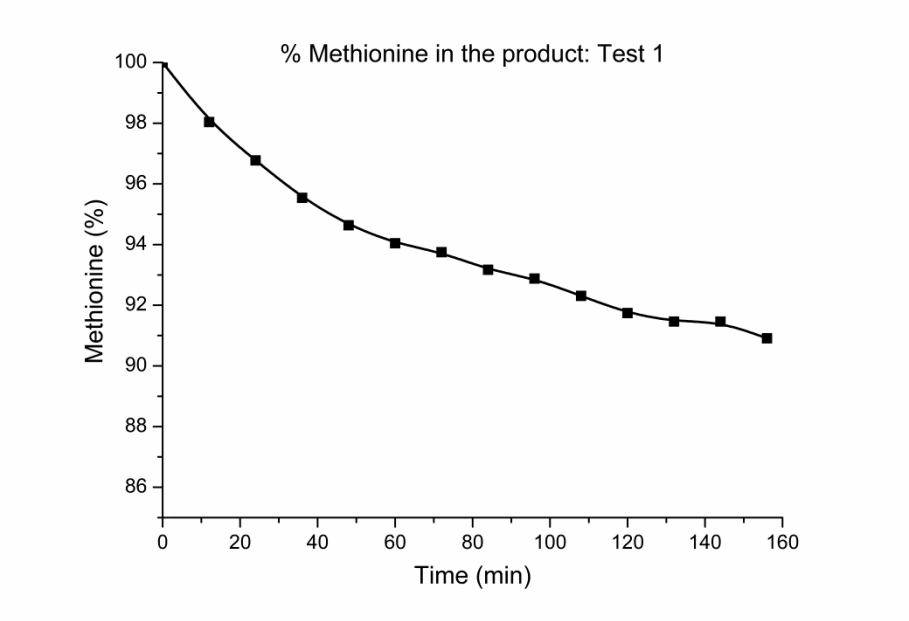

Figure 45. % of the resulting methionine in the product for the Test 1

5.1.2 Test 2

The second test is identical to the first except that the LEDs are positioned more perpendicular to the windows of the reactor. This allows light to illuminate the photosensitizer with a better angle. Results are shown in Figure 46.

The first observation is that, in comparison to the first test, the steady state is reached faster. After 1 hour a more or less constant value of resulting Met is reached, 89.3%, meaning that 10.7% conversion is achieved. This value is higher than in the first test and that means that the tested lamp configuration is better than the configuration where the lamps are in a “X” shape.

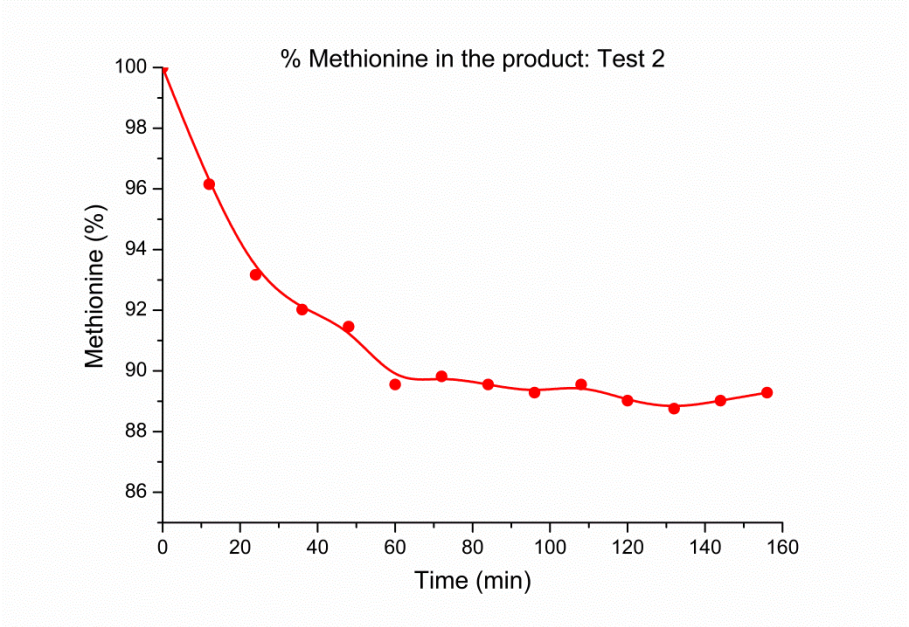

Figure 46. % of the resulting methionine in the product for the Test 2

5.1.3 Test 3

The third test is identical to the second, except that a higher air flow rate is used, hoping that thanks to this a higher amount of oxygen could be dissolved in the liquid and so increase the $^1O_2$ production. The results are available in Figure 47.

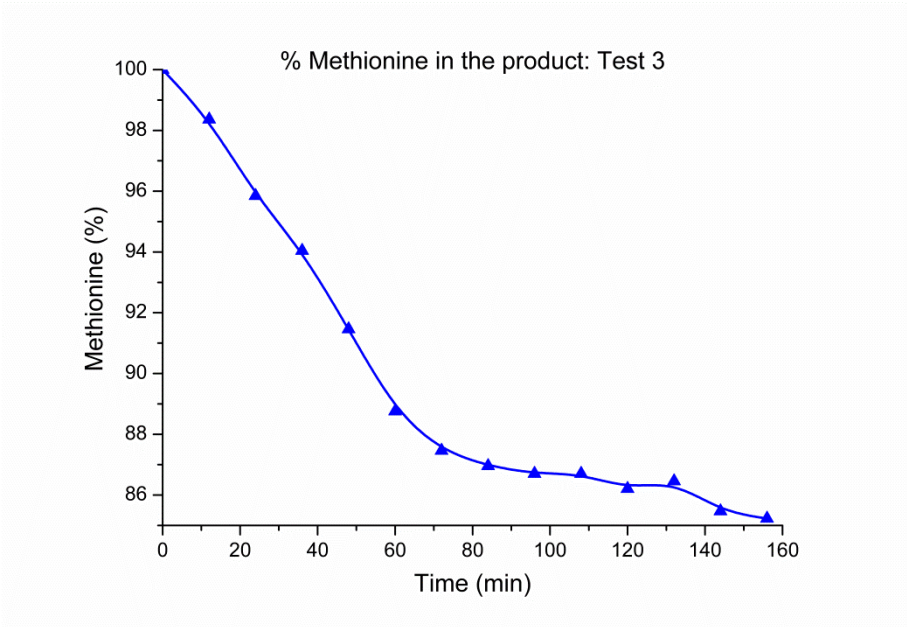

Figure 47: % of the resulting methionine in the product for the Test 3

It can be noticed that, like in the second test, steady state is achieved relatively fast: After approximatively 80 minutes a more or less constant value of 86.25 % of resulting Met is obtained, meaning a conversion of 13.75%, even if for the last two samples a conversion of 14.65% has been reached. This conversion values are, whatever, better than in the two first tests, meaning that

working with a higher air flow helps to reach better conversion, probably because more oxygen is dissolved in the liquid. This is the reason why in the last test a 20 ml/min of gas flow is chosen.

5.1.4 Test 4

Finally, the last test that has been studied with the mesoreactor is identical to the third, except that the source of oxygen for the reaction has been changed. Instead of using air, pure oxygen is used. This is again done with the hope to further increase the mass transfer and dissolution of oxygen in the liquid. The other option to increase the mass transfer in the mesoreactor, increasing pressure, was not possible with the mesoreactor, for the reasons already explained in chapter 4. Results are available in Figure 48.

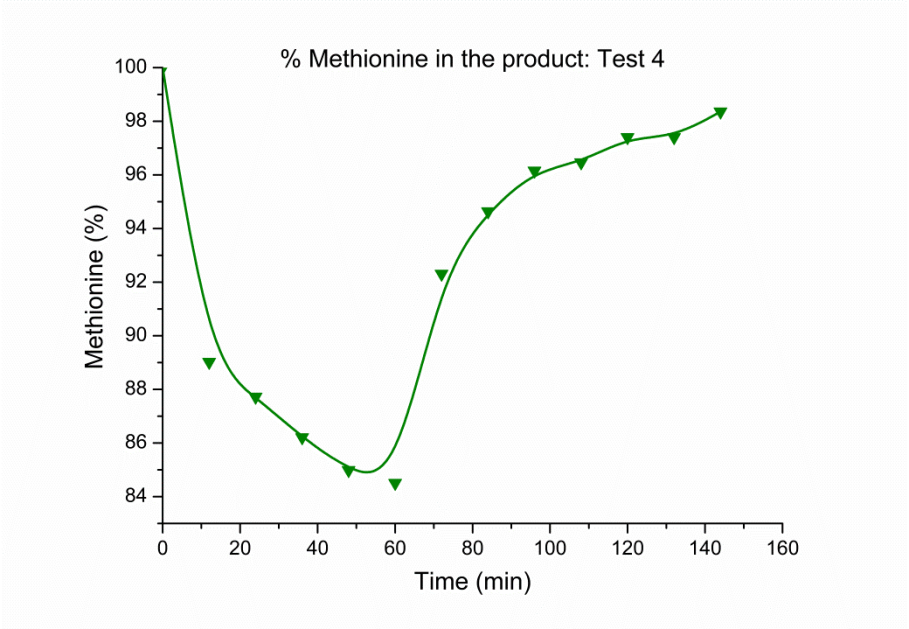

Figure 48. % of the resulting methionine in the product for the Test 4

The first thing that can be observed is that the curve has a completely different shape than the 3 previous tests. First of all, conversion of 11% is obtained after only 12 minutes. After 60 minutes the conversion reaches even 15.5%. After that, it can be seen that the conversion dramatically decreases. This can be explained when looking at the glass slides (Figure 49): The glass slide, after the reaction, is almost white, meaning that the vast majority of the RB has been degraded, a phenomena known under the name "bleaching". This means that the $^1O_2$ production is so high that not only the Met is oxygenized, but also that the photosensitizer, RB, is destroyed. Without RB, there is no $^1O_2$ production anymore, and that explains the decrease in Met conversion.

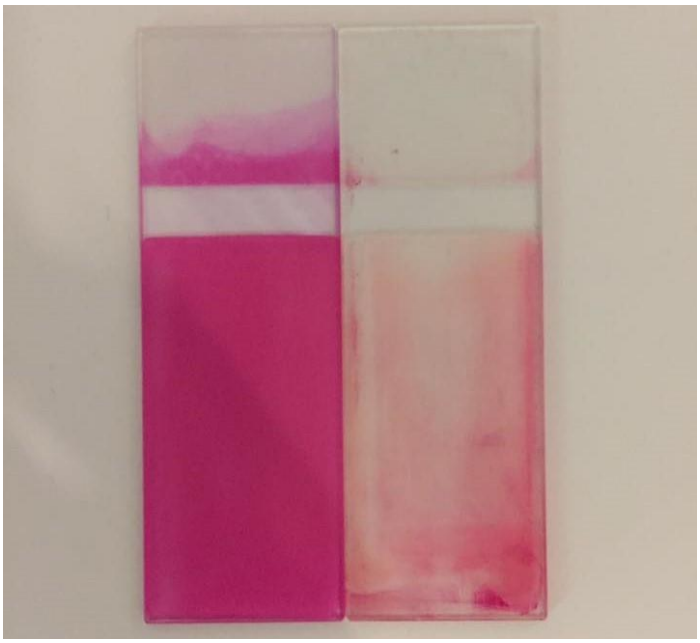

Figure 49. Initial RB glass slide (left) versus glass slide after test 4 (right)

5.1.5 Summary and Conclusion

4 tests have been studied with the mesoreactor, and in each test one parameter was changed in order to analyze its influence on the Met conversion. The results of the 4 tests can be seen on the same graph in Figure 50.

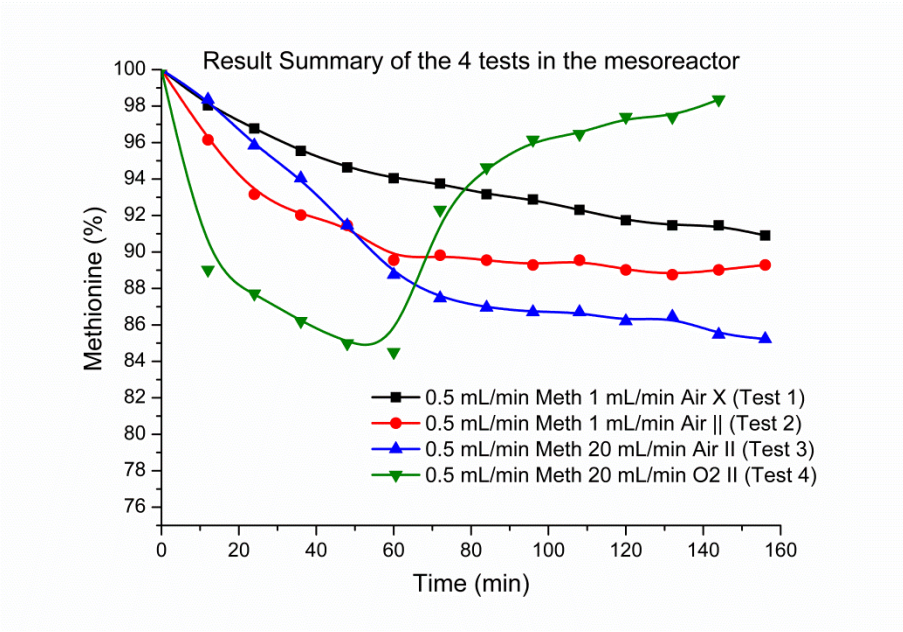

12

Figure 50. % of the resulting methionine in the product for the 4 tests

The first conclusion is that working with the LEDs in perpendicular position to the reactor windows improves the conversion. So the distance photosensitizer to lamp, and the illuminating angle plays an important role in the processes. Also working with a higher gas flowrate improves the conversion. Finally, switching from air to pure oxygen as oxygen source increases the conversion of

Met. The $^1O_2$ production, and the exposition of RB to it, is so high, that it degrades the RB. Pure oxygen will be kept as the gas for the rest of the work, because the goal of the work was to maximize the $^1O_2$ production. The objective was then to stabilize the RB in order to avoid, or at least slow down, the degradation of the photosensitizer. This is the main reason why mesoporous SiO_2 NPs were synthetized (section 2.2) and characterized (chapter 3). To be sure that the discoloration of the glass slides is really due to degradation by $^1O_2$ production and not of abrasion due to repeated flow of gas and liquid, or whatever reason, a new series of tests has been done: 2 glass slides were used to run the reactor, in the same conditions (similar to the conditions in test 4), one with the LEDs switched on, and another one with the LEDs switched off, so that $^1O_2$ production can be avoided. The results can be seen in Figure 51.

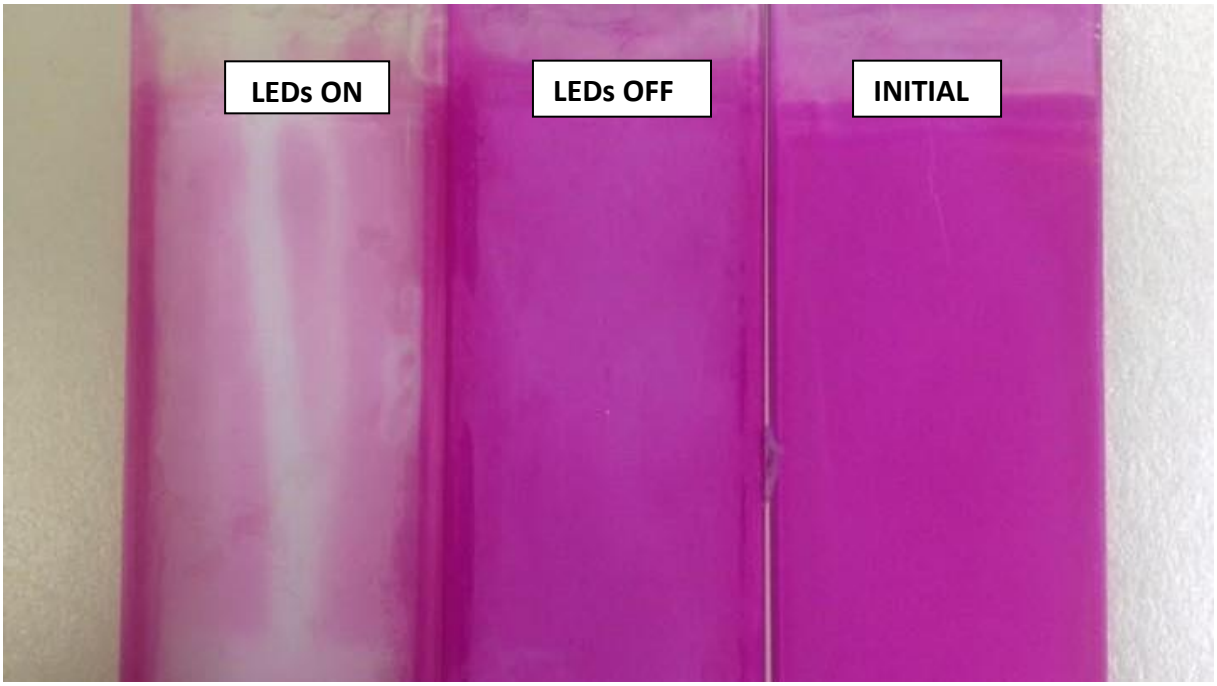

Figure 51. Comparison of the aspect of glass slides with the effect of the LEDs

It can be seen that, while the glass slide on the left, which was irradiated with green LEDs is almost white, the glass slide in the middle, which was used without LEDs, has almost no color change. The slight color change can be explained by the fact that the slide was illuminated during more than 2 hours, while the reactor was running, by natural light coming from the outside, because the test was not carried out in complete dark. This is again a proof that the RB is degraded by $^1O_2$ and so that the $^1O_2$ production is already pretty good.

5.2 Microreactor

In the case of the microreactor, like already mentioned in chapter 4, different series of tests have been carried out, in order to study the influence of 4 parameters (length of reactor, RB concentration, pressure, and flow rate) on the reaction. 3 of the series have been done with both particles coupled with RB by EDC or HATU. Indeed, in chapter 3, it has been concluded that some differences are observed between both coupling agents during the characterization. It was so interesting to see if it also results in differences for the performances.

3 main effects are investigated in the results: First of all, like for the mesoreactor, the achieved conversion of Met for the different parameters is measured. Additionally, because it was the biggest issue for the mesoreactor, the degradation in function of the parameters was analyzed. To do so, the absorbance of the solution that was injected into the reactor was measured and compared to the absorbance of the solution coming out of the reactor (once steady-state was reached). Finally, it has been tried to bring out some kinetic constants. To do so we started with the mass balance of an isothermal plug flow reactor:

$$\tau_0 = C_{L_0} * \int_0^{f_s} \frac{df}{r(f)} \quad [54]$$

where τ_0 (s) is the residence time, C_{L_0} (mol/L) the initial concentration of the limiting reagent, f_s the final conversion (-), and $r(f)$ (mol*L^{-1}*s^{-1}) the reaction rate. The reasons why the reactor is considered as isothermal and as plugflow model is developed in chapter 1. The main reasons are the important surface allowing fast heat transfer, and the segmented flow avoiding back-mixing. Following hypotheses have then been made:

- The reaction order is of first order regarding Met concentration and regarding $^1O_2$ concentration
- The concentration of $^1O_2$ is proportional to the concentration of oxygen dissolved in the water, which is again proportional to the pressure in the reactor (Henry's law)
- Because of the high oxygen flowrate and the good mass transfer due to the segmented flow, the oxygen concentration in the liquid is considered as constant, so that the reaction rate becomes a pseudo first order reaction, where the Met is the limiting reagent.

The mass balance can thus be rewritten as:

$$\tau_0 = C_{L_0} * \int_0^{f_s} \frac{df}{r(f)} = C_{L_0} * \int_0^{f_s} \frac{df}{\alpha * C_L(f)} = C_{L_0} * \int_0^{f_s} \frac{df}{\alpha * C_{L_0} * (1-f)} = \int_0^{f_s} \frac{df}{\alpha * (1-f)}$$

where f is the conversion, and α the product of the real kinetic constant, the oxygen concentration (considered as constant) and the proportionality constant between oxygen and $^1O_2$.

It is so possible to determine α. The residence time has to be recalculated for almost each experience, given that it changes for different reactor lengths, different flow rate, and different pressure (oxygen volume flowrate changes with the pressure). Henry's law predicts a higher oxygen concentration in the water when working under higher pressure, which has also to be taken into account. To do so, two new constants are introduces: β which is the kinetic constant obtained above (α) divided by the RB concentration, in order to get a kinetic constant per mole of RB; and γ which is the just introduced kinetic constant (β) divided by the pressure in the reactor, in order to make the kinetic constant independent of the pressure and so oxygen concentration.

5.2.1 Series 1 – Variation of the reactor's length

For this experiment 2 different lengths have been tested: 2 meters and 4 meters. Only the NPs coupled with RB by EDC have been tested. Results of conversion are available in Figure 52.

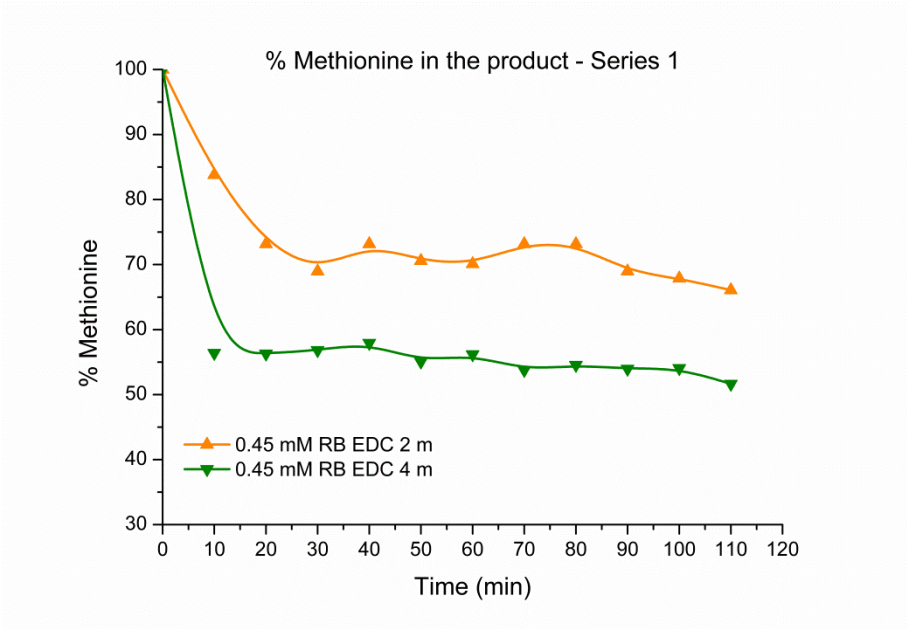

Figure 52. % of the resulting methionine in the product for the series 1

The first observation that can be made is that, compared to the mesoreactor, the conversion becomes faster constant: steady-state is reached at 20 minutes for the 2 meter reactor while it is already achieved at 10 minutes for the 4 meter microreactor. It can also be seen that the conversion is higher when using the 4 meter reactor than when using the 2 meter reactor. This seems logical because the residence time is doubled when using a 2 times longer reactor. Conversion oscillates around 33% for the 2 meter reactor, while a 46% conversion is reached with the 4 meter reactor.

The degradation of the SiO_2-RB NPs was also measured during the reaction. Without big surprise the degradation was higher for the 4 meter reactor than for the 2 meter reactor. Once again this can be explained with the residence time difference. The particles were illuminated during a two times longer time period with the 4 meter reactor. The absorbance, and so the RB amount, was reduced by 23% in the case of using 2 meters, and by 45% using 4 meters. These results are coherent with the illumination time, a 2 times longer light exposure leads to a 2 times higher degradation.

Finally, the modified kinetic constants α, β, and γ, introduced above can be calculated. To do this, the residence time of both reactors has to be known. The inlet liquid flowrate was of 0.5 ml/min, while the gaseous flowrate was of 15 mL/min, at atmospheric pressure. At 6.9 bars, the oxygen is compressed, and the flowrate only corresponds to 2.20 mL/min. This gives a total reagent inlet flowrate of 2.7 mL/min. The 2 meter reactor has a volume of 1 mL, leading to a residence time of 22.22 s, while the 4 meter reactor and its 2 ml volume has a residence time of 44.44 s. It is possible to calculate these 3 constants having the residence times and the final conversion. They are listed in Table 3.

Reactor length (m)	f_s	τ_0 (s)	[RB] (mM)	P (bar)	α (s^{-1})	β (s* mM)$^{-1}$	γ (s* mM*bar)$^{-1}$
2	0.33	22.22	0.45	6.9	0.0180	0.04	$5.797*10^{-3}$
4	0.46	44.44	0.45	6.9	0.0139	0.0309	$4.477*10^{-3}$

Table 3 : kinetic constants calculated for different lengths of the reactor

The first thing that is noticed is that the kinetic constants are not the same, even if they should: In fact all what has been modified is the residence time which has no influence on the kinetic constant. Nevertheless this result can be explained: In the 4 meter reactors the RB NPs are exposed to light during a two times longer time period. During this time they undergo more degradation. So their efficiency will decrease all along the reactor, which explains the smaller value for the kinetic constant.

5.2.2 Series 2 – Variation of the RB concentration

For this experiment, 3 different concentration of RB have been tested: 0.45 mM, 0.9 mM and 1.35 mM. NPs coupled with RB by the two different coupling agents, EDC and HATU, have been tested. Results for the conversion of Met are shown in Figure 53, while results for the degradation of the RB are shown in Figure 54.

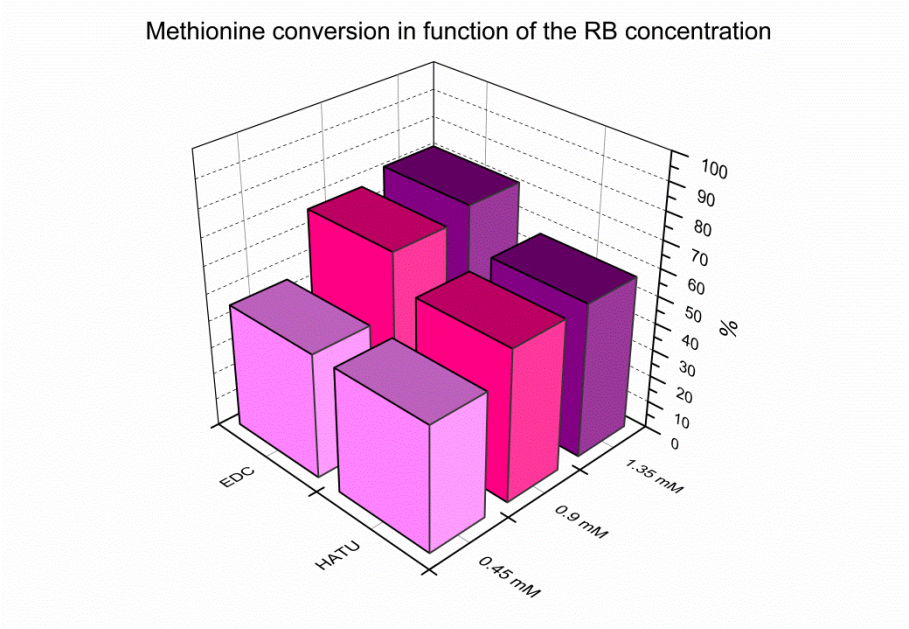

Figure 53. Methionine conversion as a function of the RB concentration for NPs coupled by both EDC and HATU

Regarding the conversion it can be seen that the EDC has a better efficiency compared to the HATU: While the conversions are of respectively 46%, 68%, and 72% for the 0.45mM, 0.9 mM and 1.35 mM for the NPs coupled with EDC, the conversions for the same RB concentration are of only 46%, 56% and 57% when using HATU. Additionally it can be observed that the conversion increases between 0.45 mM and 0.9 mM, for both types of particles, but that there is almost no increase between 0.9 and 1.35 mM. This can be explained with the light penetration (Figure 55 and 56). While for both type of particles the light penetrates to more than 50% to the center of the reactor when the concentration is 0.45 mM, it doesn't reach 50% anymore when the concentration is 0.9 mM, and is in particular low when the concentration increases to 1.35 mM. This can explain why there is no significant conversion difference between the 0.9 mM and the 1.35 mM test. Despite having theoretically more RB molecules available to produce $^1O_2$, the light doesn't penetrate enough to excite them all. A maximum is reached. Also the lower conversion for the NPs coupled by HATU can be explained this way. Their absorbance coefficient is higher than for the particles coupled by EDC, so light penetrates more difficultly at high concentrations and so the conversion can't increase.

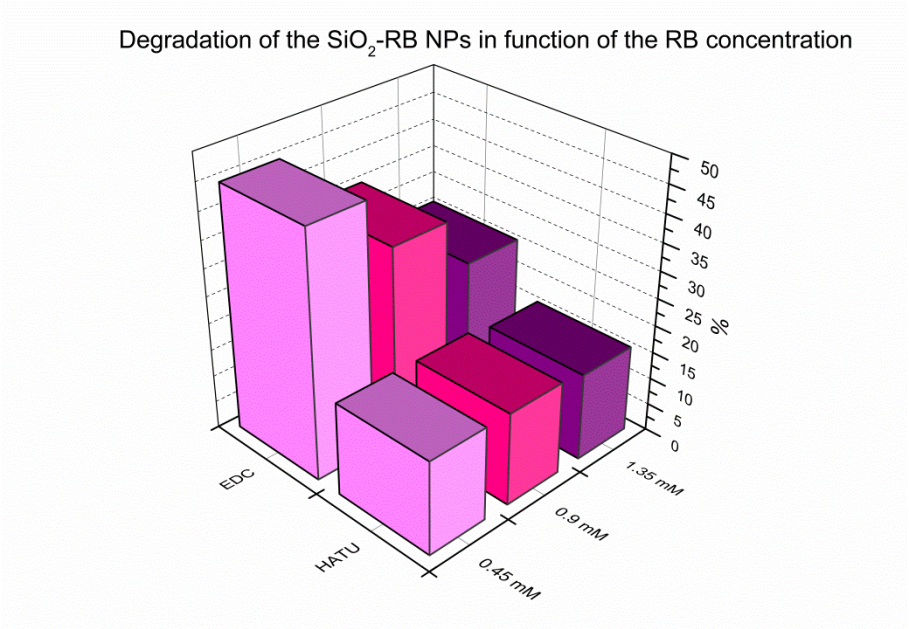

Figure 54. RB degradation as a function of the RB concentration for NPs coupled by both EDC and HATU

The results of the degradation are also interesting. While the NPs coupled by EDC showed a predictable behavior, the particles coupled by HATU do not. When EDC is used, the degradation decreases with increasing RB concentration, which can be easily explained by the fact that if a same quantity of RB is degraded, its relative importance will decrease if there are more particles. The degradation is 45, 35.3 and 25.9% for the 0.45, 0.9 and 1.35 mM concentrations, respectively. When HATU is used this is not observed anymore, the degradation is almost constant and identical for each concentration: 17.1, 17 and 17% for the same concentrations. It looks like a maximum of degradation is reached around 17%, and would mean that coupling RB to SiO_2 NPs with HATU leads to a stronger and more stable configuration.

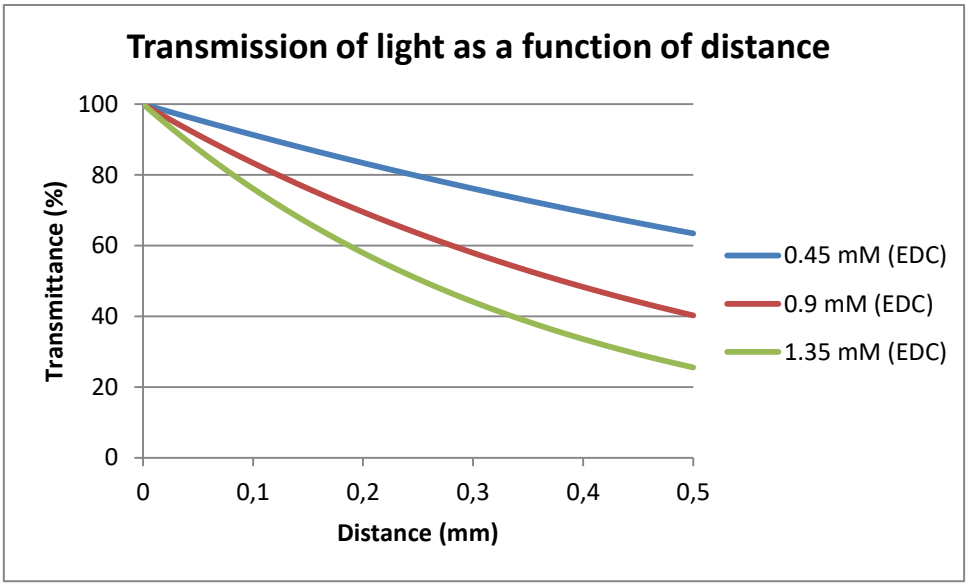

Figure 55. Light transmission as a in function of the distance for different RB-SiO_2 NPs coupled by EDC

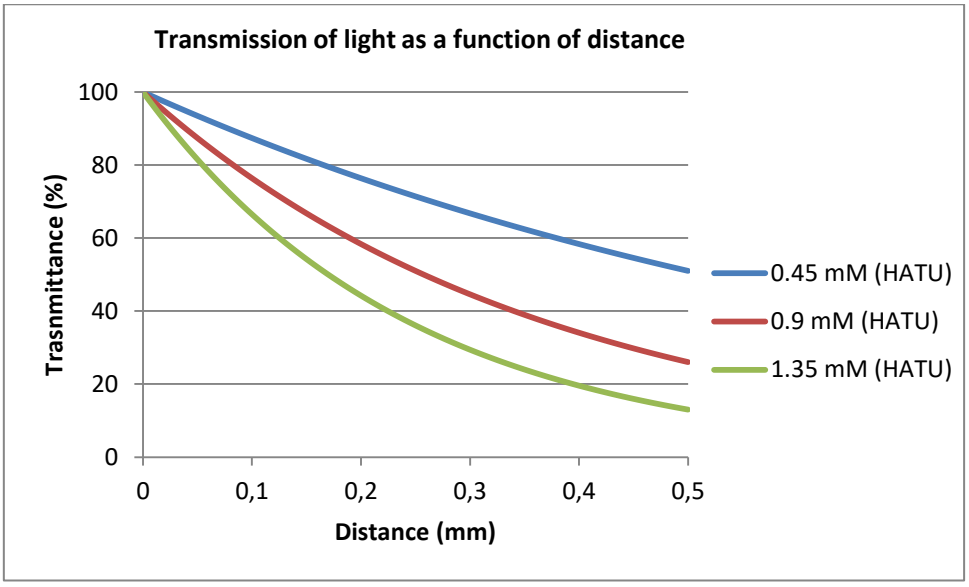

Figure 56. Light transmission as a function of the distance for different RB-SiO_2 NPs coupled by HATU

These graphs were obtained by measuring the extinction coefficient of the different particles using the spectrophotometer. To do so, the absorbance of different known concentrations were measured and the coefficient obtained by linear regression. Then the results were plotted using the formula of transmission:

$$T(\%) = 100 * 10^{-\varepsilon * L * C}$$

where ε is the molar extinction coefficient of the sample, L the length of the sample, and C the concentration of the sample.

Finally the kinetic constants can be calculated. The residence time is the same than the 4 meter reactor (44.44 seconds) in the first experiment, given that neither the volume, the flowrates nor the pressure change. Results are listed in Table 4.

Coupling agent	f_s	τ_0 (s)	[RB] (mM)	P (bar)	α (s^{-1})	β (s* mM)$^{-1}$	γ (s* mM*bar)$^{-1}$
EDC	46	44.44	0.45	6.9	0.0139	0.0301	$4.477*10^{-3}$
EDC	68	44.44	0.9	6.9	0.0256	0.0284	$4.116*10^{-3}$
EDC	72	44.44	1.35	6.9	0.0286	0.0212	$3.072*10^{-3}$
HATU	46	44.44	0.45	6.9	0.0139	0.0301	$4.477*10^{-3}$
HATU	56	44.44	0.9	6.9	0.0185	0.0206	$2.986*10^{-3}$
HATU	57	44.44	1.35	6.9	0.0190	0.0141	$2.043*10^{-3}$

Table 4 : kinetic constants for both coupling agents calculated when varying the RB concentration

The results confirm what has already been discussed above. The kinetic constant increases with the concentration of RB, because more molecules of photosensitizer are available. However, the second kinetic constant, which is divided by the RB concentration to have a result per mol of RB, shows a decrease, due to the light penetration. This theory of light penetration is confirmed when looking at the results of the 1.35 mM concentration of EDC particles and at the 0.9 mM concentration of the HATU particles. If the transmission of light of these two situations is observed on Figure 55 and 56, it can be seen that the curves are almost identical, because the particles coupled by HATU have a stronger absorbance (Figure 34). Interestingly enough not only the transmission of light for these particles are almost identical, but also their kinetic constants (the ones weighted by their RB concentrations, β and γ) are similar.

5.2.3 Series 3 – Variation of the liquid flowrate

During this test, 3 different liquid flowrates were tested, 0.25 mL/min, 0.5 mL/min, and 0.75 mL/min, while keeping the oxygen flowrate constant. In the same way than for the previous test, both NPs coupled with RB by EDC and by HATU were tested. Results of conversion are shown in Figure 57 and results of degradation are shown in Figure 58.

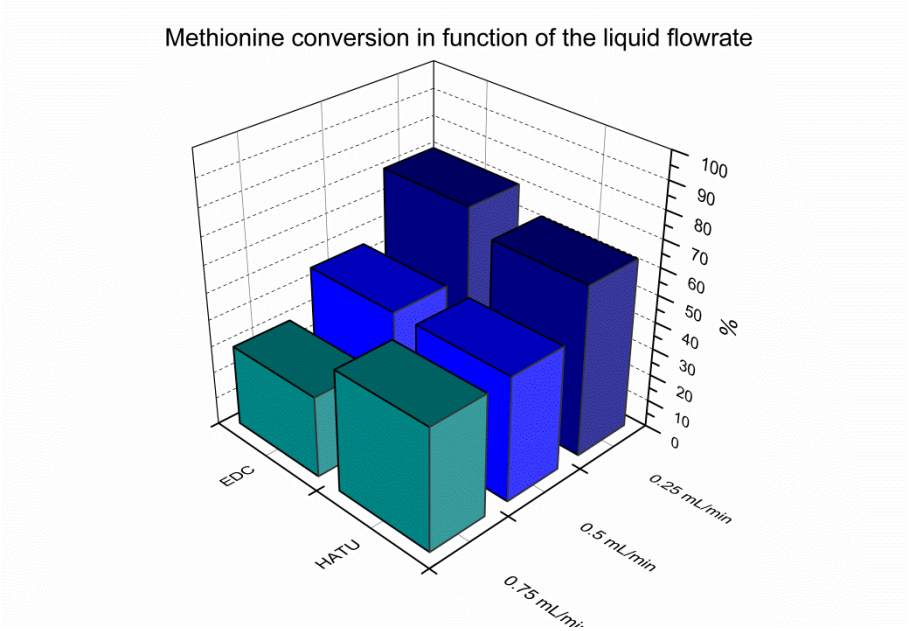

Figure 57. Methionine conversion as a function of the liquid flowrate for NPs coupled by both EDC and HATU

Regarding the conversion there are two major observations that can be made: first of all the conversion increases when the liquid flowrates decreases. This sounds logical because smaller

flowrates lead to higher residence times and so to longer reaction times. The second remark is that it is, in this case, difficult to distinguish which particles are the most efficient: At the intermediate flowrate (0.5 mL/min) both conversion are identical at 46%. At the lower flowrate (0.25 mL/min), both reaction lead to a higher conversion, but the efficiency of the particles coupled with RB by EDC is increased in comparison to the NPs used with HATU(71% conversion with the EDC versus 63% with the HATU). With the higher flowrate (0.75 mL/min) it is the opposite, conversions for both types of particles decrease, but the particles coupled with EDC this time loose efficiency in comparison to the NPs functionalized by HATU: 30% conversion with EDC versus 45% with HATU.

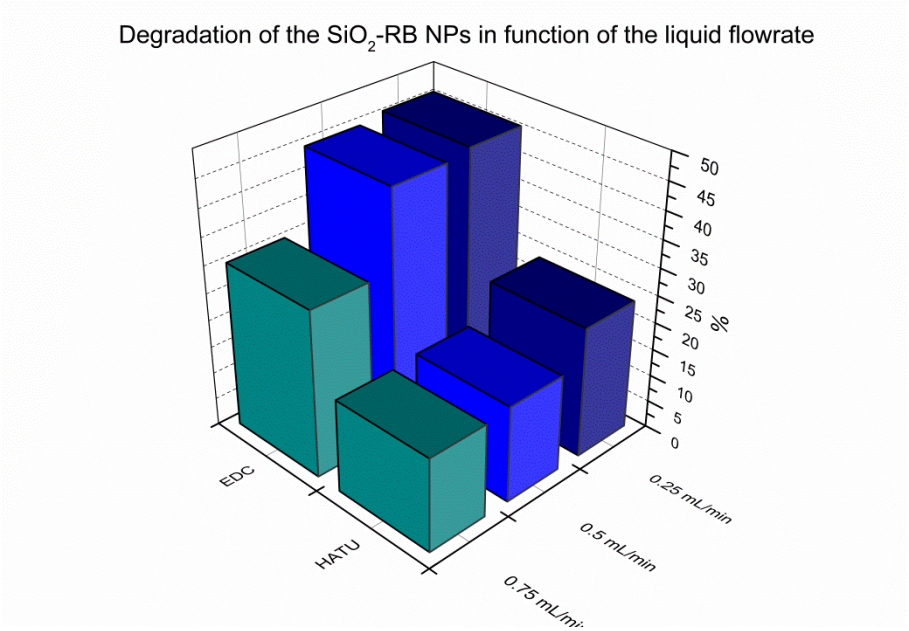

Figure 58. RB degradation in function of the liquid flowrate for NPs coupled by both EDC and HATU

Concerning the degradation, the trend observed in the last test seems to be confirmed also this time. NPs coupled with RB by HATU degrade less fast and seem more stable than the ones coupled with EDC. The degradation is more or less doubled with EDC compared to HATU. Degradation is 30.6% versus 17.1% for the 0.75 mL/min flowrate, 45% versus 17.7% for the 0.5 mL/min flowrate, and 46% versus 24% for the 0.25 mL/min flowrate. The increasing degradation with smaller flowrates can be explained again by larger residence times. It also seems that a maximum of degradation is reached, around 45-46% for the NPs coupled with EDC, because there is no significant degradation difference for these particles between the 0.5 mL/min and the 0.25 mL/min liquid flowrate.

Finally the 3 different kinetic constants can be calculated. To do so, this time new residence times have to be calculated. The pressure and gas flowrate don't change, meaning that they still account for 2.20 mL/min. Total reagent flowrates are thus of 2.45 mL/min, 2.70 mL/min and 2.95 mL/min, leading to residence times of 48.98 s for the smaller liquid flowrate, 44.44 s for the intermediate flowrate, and 40.68 for the higher flowrate. Results are listed in Table 5.

Coupling agent	f_s (-)	τ_0 (sec)	[RB] (mM)	P (bar)	α (s^{-1})	β (s* mM)$^{-1}$	γ (s* mM*bar)$^{-1}$
EDC	71	48.98	0.45	6.9	0.0253	0.0562	$8.145*10^{-3}$
EDC	46	44.44	0.45	6.9	0.0139	0.0309	$4.477*10^{-3}$
EDC	30	40.68	0.45	6.9	0.0088	0.0196	$2.841*10^{-3}$
HATU	63	48.98	0.45	6.9	0.0203	0.0451	$6.536*10^{-3}$
HATU	46	44.44	0.45	6.9	0.0139	0.0309	$4.477*10^{-3}$
HATU	45	40.68	0.45	6.9	0.0147	0.0327	$4.739*10^{-3}$

Table 5: kinetic constants for both coupling agents calculated when varying the liquid flowrate

The calculated kinetic constants show that the reaction is faster when smaller liquid flow rates are used. So the increase of the conversion is not only due to the longer residence time but also due to the kinetics. This could be explained by two different factors: First, when mixing the liquid and the gas together before injecting in the reactor, having smaller flowrates could increase the mixing efficiency and so the mass transfer from oxygen into the liquid phase. Also, by diminishing the liquid/gas ratio, smaller liquid segments are formed and that can again increase the mass transfer of the oxygen into the liquid phase. When using higher liquid flowrates the kinetics, at least for the NPs coupled by EDC, decrease and could again be explained by mixing efficiency and liquid segments lengths. Just for NPs coupled with HATU there is no significant difference observed between the higher liquid flowrate and the intermediate one. The kinetics is even a little bit higher for the 0.75 mL/min flowrate. This error could be explained by the accuracy of NMR to differentiate two similar conversions, because no other logical explanation could be found.

5.2.4 Series 4 – Variation of the pressure

For this last test, two different pressures were tested: 6.9 bars and 8.5 bars, which was the maximal pressure that could be used. Working at higher pressure did not allow a good mixing and a segmented flow. Increasing the pressure was made with the hope to increase the quantity of oxygen dissolved in the liquid and so accelerate the reaction. Again, like in the two previous tests, both NPs coupled with RB by EDC and by HATU have been tested. Results of conversion are shown in Figures 59 and 60. Results of degradation are shown in Figures 61 and 62.

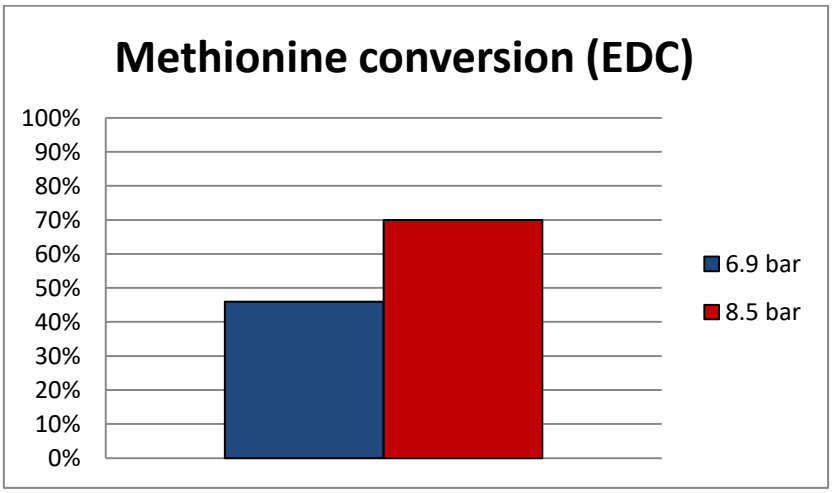

Figure 59. Methionine conversion as a function of the pressure for NPs coupled by EDC

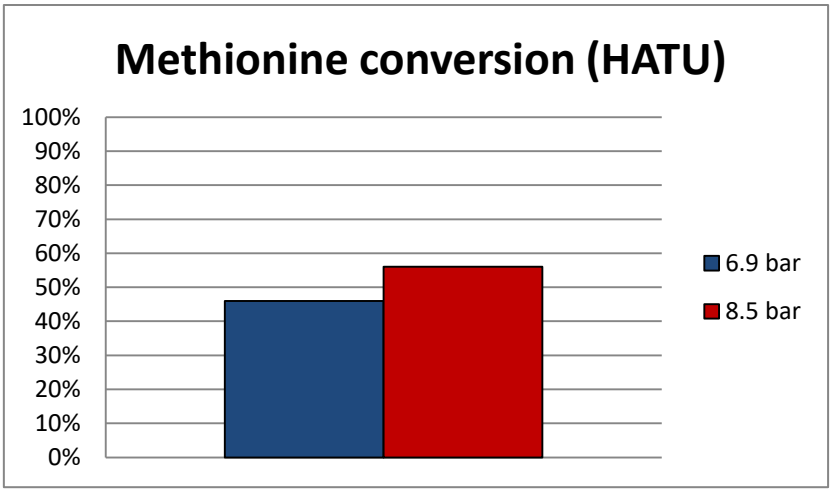

Figure 60. Methionine conversion as a function of the pressure for NPs coupled by HATU

Concerning the conversion, two major observations can be made: First, the conversion increases with the pressure. This can be explained on one side by the fact that the residence time increases, due to the compression of the gaseous phase, and on the other side by Henry's law that states that at higher pressure more oxygen is dissolved in the liquid. The second observation is that at higher pressure the efficiency of the SiO_2 NPs coupled with RB by EDC is higher than the NPs coupled by HATU. At 6.9 bar both have a conversion of 46%, while at 8.5 bar the NPs coupled with EDC convert 70% of the methionine and 56% of conversion is achieved when using HATU.

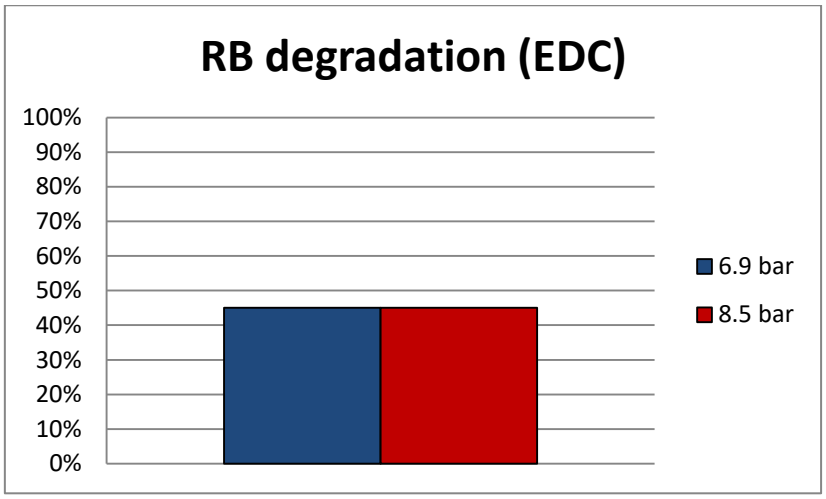

Figure 61. RB degradation as a function of the operating pressure for NPs coupled by EDC

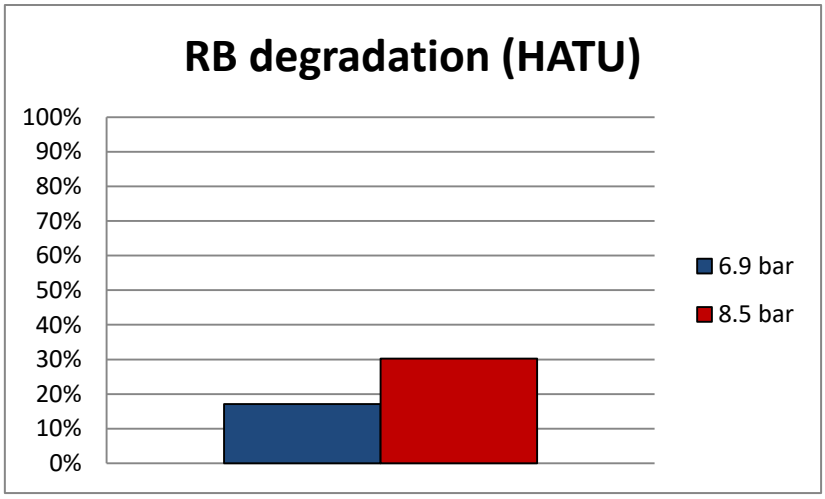

Figure 62. RB degradation as a function of the operating pressure for NPs coupled by HATU

Concerning the degradation of the RB, again two major observations can be made: First, like in the previous tests, the degradation is higher for the NPs coupled by EDC. Secondly, like already observed at the previous test, the particles functionalized by EDC seem to have reached a maximum of degradation, because the degradation does not increase when the pressure is increased. Degradation were 45% at both pressures when using EDC, while when using HATU the degradation was of 17% at the pressure of 6.9 bar and of 30% at the pressure of 8.5 bar.

Finally, the 3 different kinetic constants were again calculated. To do so, again, new residence times had to be calculated. The reactor length was still of 4 meters, meaning a volume of 2 mL, and the liquid flow rate of 0.5 mL/min. The liquid being considered as incompressible, just the gaseous volume changes with the pressure. A 15 mL/min, at atmospheric pressure, flowrate of oxygen corresponds so to a 1.79 mL/min flowrate at 8.5 bar. This results so in a total flowrate of 2.29 mL/min for the reagents and so a residence time of 52.40 s. Results are listed in Table 6.

Coupling agent	f_s	τ_0 (sec)	[RB] (mM)	P (bar)	α (s^{-1})	β (s* mM)$^{-1}$	γ (s* mM*bar)$^{-1}$
EDC	46	44.44	0.45	6.9	0.0139	0.0309	$4.477*10^{-3}$
EDC	70	52.40	0.45	8.5	0.0230	0.0511	$6.012*10^{-3}$
HATU	46	44.44	0.45	6.9	0.0139	0.0309	$4.477*10^{-3}$
HATU	56	52.40	0.45	8.5	0.0157	0.0349	$4.106*10^{-3}$

Table 6 : kinetic constants for both coupling agents calculated when varying the liquid flowrate

It can be seen that, obviously, the two first constants are higher when working under higher pressure. This is due to the fact that more oxygen is dissolved in the liquid. In the other hand, two opposed phenomena are observed when the constant is divided by the pressure to make them independent (last constant). For the NPs coupled with EDC the constant is higher than at low pressure. This could be explained by, for instance, a better mixing at higher pressure. On the other side, when HATU is used, a lower kinetic constant is obtained. This could be explained by the fact that it takes more time to dissolve enough oxygen to reach saturation pressure in the liquid du. So in fact, two opposed phenomena are observed and so two different explanations. New tests should be performed to know which trend can be confirmed.

5.2.5 Summary and conclusion

In this section, different parameters have been tested in order to determine the optimal conditions to run the microreactor, the parameters that allow to maximize the kinetics and the conversion (and so the production of $^1O_2$), while protecting and preserving the maximum the SiO_2 - RB NPs.

To do so, the most interesting is to work with a low liquid flowrate. It allows a much better mixing and so a much better mass transfer of the oxygen into the liquid. The only drawback is the productivity decrease when working with low flowrates. Also it is recommended to not work with too high SiO_2-RB NPs concentration. The light penetration counterbalances the high amount of RB. Also the cost, when working with more NPs, increases. It is much more interesting to work with a smaller concentration, like the one that has been used the majority of the time in this work (0.45 mM of RB) but longer residence times. Working at higher pressures allows a higher concentration of oxygen into the liquid. The reactor should so be operated at a pressure as high as possible, even if some mass transfer problems could appear, like observed with HATU. Nevertheless, working at high pressure remains advantageous. Finally, when these 3 parameters have been set, the desired conversion can simply be achieved by varying the length of the reactor and so its residence time.

Concerning the coupling agents, there are two points of view: Working with HATU seems to allow a slightly faster conversion and kinetics. On the other side, the NPs coupled with HATU have a much better stability and undergo bleaching much more slowly. For this reason, working with HATU seems more interesting. The protection of the RB was the first goal of the synthesis of the mesoporous NPS. If the conversion wants to be increased, a simple increase of the length of the reactor, resulting in a higher residence time, does the job. Protecting and preserving the RB, is much more complicated and more complex. The SiO_2 NPs coupled with RB by HATU clearly showed the most promising results, and that is the reason why HATU will be considered as “the champion”.

6. Conclusion & perspectives

The goal of this work was the optimization of a microreactor in order to achieve photooxygenation of Met. This reaction was selected to point out the production of $^1O_2$. To do so, a photosensitizer, RB, was coupled to SiO_2 NPs. Different types of particles have been synthetized, characterized and tested. Two different reactors have been run, and different parameters have been adjusted. At the end, the initial goal has been achieved, when looking at the results obtained at the end of the work, where relatively good conversions of Met were obtained.

In the first chapter, the importance of photooxygenation in photodynamic therapy, depollution, and synthesis has been highlighted. The production of $^1O_2$ has also been defined. Finally, the advantages of working with microreactors, like light penetration, or excellent mass and heat transfer have been described.

In the second chapter different SiO_2 NPs have been synthetized: Dense particles that were incorporated into a TiO_2 matrix to form a coating for the mesoreactor, but also microporous particles and mesoporous particles. Also the two main coupling agents, EDC and HATU, and the way how the coupling had to be performed were described.

The third chapter was dedicated to the characterization of the particles and coatings obtained in the previous chapter. To do this, profilometry was conducted on the coatings to measure their thickness and roughness, thermogravimetric analysis was performed on the particles to measure their RB loading, UV-visible absorbance was carried out to determine the maximum absorbance test and to differentiate the particles obtained by different coupling agents, and the characterization was completed with a BET analysis to obtain isotherms, surface area and pore volumes of the different particles. The mesoporous SiO_2 NPs showed clearly the most promising results, with a large surface area and sufficient pore volume, allowing attaching an important amount of RB. This was also confirmed by the TG analysis. Finally, the UV-visible analysis, and the pore volume obtained by BET, allowed differentiating particles with RB by EDC or HATU.

In the fourth chapter, both the mesoreactor and the microreactor, and all the equipment needed to run them, were described. All the tests that were carried out were explained and justified. Finally, the LEDs used for the reaction were characterized and the solvent choice, water, was justified.

The last chapter explained all the results obtained. The microreactor didn't succeed well because of the fast bleaching of the RB-SiO_2 particles in the coating. The microreactor allowed reaching promising results. Different parameters were tested in order to find the optimal conditions: It has been concluded that working with a low liquid flowrate allows better mixing, the concentration of RB should not be too high to get rid of the light penetration issues, and working at the highest possible pressure to allow a better oxygen concentration in the liquid phase. Some kinetic constants could also be determined thanks to the plug flow reactor model. Finally, the degradation of RB has been measured.

The conclusion of this work is that, even if slightly better kinetics and conversion were obtained for the NPs coupled with RB by EDC, HATU is the most interesting coupling agent. The conversions were only slightly lower but the degradation of the RB, the stability of the particles, was

much better. So, at this point, one coupling agent has to be chosen to continue the work on this project, and HATU is recommended.

The goal of this project, to work on the optimization of the reaction in the microreactor, has been was reached given that conversion of more of 70% were reached in some conditions. Nevertheless, like always, the optimization could be further increased.

First of all, for time reasons, only the influence of some parameters was tested on the reaction. Some other parameters, like for instance the oxygen flow rate, the use of other solvents (even if the "green and sustainable" aspect of the project would be lost) can be tested. Also, for each parameter, the optimal condition was determined; it would be interesting to run the reactor with all these optimal conditions gathered together.

Then, it would be interesting to recover the particles introduced into the reactor, through for instance centrifugation, and trying to reuse them. It could so for instance be seen if the particles reach a maximum of degradation, maximum that could correspond to the RB attached at the surface of the particles, and so having the RB in the pores protected from bleaching and degradation.

Additionally, it could be interesting, once stable SiO_2 -RB nanoparticles have been obtained, to immobilize these particles on the PFA tubing of the microreactor as it has been done for the mesoreactor. It would have the advantage to skip the downstream separation process, between the liquid phase and the dispersed particles. This of course requires particular light-stable particles, because they are continuously exposed to green light.

Finally improving the couples NPs-PS is also a perspective that has to be studied. This can be done by developing core-shell structures, where the core would be made out of metal (Ag or Au). The shell, made out of silica, would allow to control the distance between the attached RB and the metal increasing the $^1O_2$ production by Localized Surface Plasmon Resonance.

Bibliography

[1] “<SC>L</SC>-Methionine M9625” in *Sigma-Aldrich.* http://www.sigmaaldrich.com/catalog/product/sial/m9625?lang=en&region=BE. Consulted on Mars 6th, 2017.

[2] “<SC>L</SC>-Methionine sulfoxide M1126” in *Sigma-Aldrich.* http://www.sigmaaldrich.com/catalog/product/sigma/m1126?lang=en&region=BE. Consulted on Mars 6th, 2017.

[3] “Rose bengal 330000” in *Sigma-Aldrich.* http://www.sigmaaldrich.com/catalog/product/aldrich/330000?lang=en&region=BE. Consulted on Mars 6th, 2017.

[4] de Souza Oliveira, R. C., Corr??a, R. J., Teixeira, R. S. P., Queiroz, D. D., da Silva Souza, R., Garden, S. J., … Ribeiro, E. S. (2016). Silica nanoparticles doped with anthraquinone for lung cancer phototherapy. *Journal of Photochemistry and Photobiology B: Biology*.

[5] Montagnon, T., Kalaitzakis, D., Triantafyllakis, M., Stratakis, M., & Vassilikogiannakis, G. (2014). Furans and singlet oxygen--why there is more to come from this powerful partnership. *Chemical Communications*, *50*(98), 15480–98.

[6] Wilkinson, F., Helman, W. P., & Ross, A. B. (1995). Rate Constants for the Decay and Reactions of the Lowest Electronically Excited Singlet State of Molecular Oxygen in Solution. An Expanded and Revised Compilation. *Journal of Physical and Chemical Reference Data*, *24*(2), 663–677.

[7] Lismont, M., Dreesen, L., Heinrichs, B., & Páez, C. (2016). Protoporphyrin IX Functionalised AgSiO2 Core-shell Nanoparticle: Plasmonic Enhancement of Fluorescence and Singlet Oxygen Production. *Photochem Photobiol*, *92*, 247–256.

[8] “IUPAC Gold Book - quantum yield, Φ” in *Goldbook.iupac.org.* https://goldbook.iupac.org/Q04991.html. Consulted on Mars 6th, 2017.

[9] Denk, M. (2000). *The Chemistry of Oxygen & Sulfur*. http://131.104.156.23/lectures/231/231_oxygen-group. Consulted on Mars 6th, 2017.

[10] Kim, H., Kim, W., MacKeyev, Y., Lee, G. S., Kim, H. J., Tachikawa, T., … Lee, J. (2012). Selective oxidative degradation of organic pollutants by singlet oxygen-mediated photosensitization: Tin porphyrin versus C60 aminofullerene systems. *Environmental Science and Technology*, *46*(17), 9606–9613.

[11] Cambi??, D., Bottecchia, C., Straathof, N. J. W., Hessel, V., & No??l, T. (2016). Applications of Continuous-Flow Photochemistry in Organic Synthesis, Material Science, and Water Treatment. *Chemical Reviews*, *116*(17), 10276–10341.

[12] Gemoets, Su, Y., Shang, M., Hessel, V., Luque, R., & Noel, T. (2016). Liquid phase oxidation chemistry in continuous-flow microreactors. *Chem. Soc. Rev.*, *45*(1), 83–117.

[13] “(3-<WBR>Aminopropyl)<WBR>triethoxysilane 440140” in *Sigma-Aldrich.* http://www.sigmaaldrich.com/catalog/product/aldrich/440140?lang=en&region=BE. Consulted on Mars 6th, 2017.

[14] “N-<WBR>(3-<WBR>Dimethylaminopropyl)<WBR>-<WBR>N’-ethylcarbodiimide hydrochloride (EDC) 98% 161462” in *Sigma-Aldrich.* http://www.sigmaaldrich.com/catalog/product/aldrich/161462?lang=en&region=BE. Consulted on Mars 6th, 2017.

[15] “HATU 445460” in *Sigma-Aldrich.* http://www.sigmaaldrich.com/catalog/product/aldrich/445460?lang=en&region=BE. Consulted on Mars 6th, 2017.

[16] J.-C. M. Monbaliu, CHIM9265-1 - Introduction to Continuous Flow Organic Synthesis : Lecture 1-6. 2016.

[17] “Perfluoroalkoxy” in *Fr.wikipedia.org.* https://fr.wikipedia.org/wiki/Perfluoroalkoxy. Consulted on Mars 7th, 2017.

[18] Wang, X. D., Shen, Z. X., Sang, T., Cheng, X. Bin, Li, M. F., Chen, L. Y., & Wang, Z. S. (2010). Preparation of spherical silica particles by St??ber process with high concentration of tetra-ethyl-orthosilicate. *Journal of Colloid and Interface Science*, *341*(1), 23–29.

[19] Jankiewicz, B. J., Jamiola, D., Choma, J., & Jaroniec, M. (2012). Silica-metal core-shell nanostructures. *Advances in Colloid and Interface Science*, *170*(1–2), 28–47.

[20] “Orthosilicate de tétraéthyle” in *Fr.wikipedia.org.* https://fr.wikipedia.org/wiki/Orthosilicate_de_t%C3%A9tra%C3%A9thyle. Consulted on April 21th, 2017.

[21] Lofgreen, J. E. (2014). Controlling morphology and porosity to improve performance of molecularly imprinted sol–gel silica. *Chem. Soc. Rev.*, *43*(3), 911–933.

[22] Doeuff, S., Henry, M., Sanchez, C., & Livage, J. (1987). Hydrolysis of titanium alkoxides: Modification of the molecular precursor by acetic acid. *Journal of Non-Crystalline Solids*, *89*(1–2), 206–216.

[23] Eshaghi, A., Pakshir, M., & Mozaffarinia, R. (2010). Preparation and characterization of TiO2 sol-gel modified nanocomposite films. *Journal of Sol-Gel Science and Technology*, *55*(3), 278–284.

[24] Yu, J., Zhao, X., & Zhao, Q. (2001). Photocatalytic activity of nanometer TiO2 thin films prepared by the sol-gel method. *Materials Chemistry and Physics*, *69*(1–3), 25–29.

[25] Jimmy, C., Yu, J., & Zhao, J. (2002). Enhanced photocatalytic activity of mesoporous and ordinary TiO 2 thin films by sulfuric acid treatment. *Applied Catalysis B: Environmental*, *36*, 31–43.

[26] Paz, Y., Luo, Z., Rabenberg, L., & Heller, a. (1995). Photooxidative self-cleaning transparent titanium dioxide films on glass. *Journal of Materials Research*, *10*(11), 2842–2848.

[27] Niederberger, M. (2009). Aqueous and Nonaqueous Sol-Gel. *Metal Oxide Nanoparticles in Organic Solvents*, 7–19.

[28] "Titanium isopropoxide' in *En.wikipedia.org.* https://en.wikipedia.org/wiki/Titanium_isopropoxide. Consulted on April 22th, 2017.

[29] Moran--Mirabal, Research, & Group. (2014). Piranha Cleaning – Glass Surfaces, 3–5.

[30] "Automatic dip coating unit - RDC 21-K - Bungard-Elektronik GmbH & Co. KG – Videos" in Directindustry.com. http://www.directindustry.com/prod/bungard-elektronik-gmbh-co-kg/product-178266-1786670.html. Consulted on April 24th, 2017.

[31] "Carbodiimide Crosslinker Chemistry | Thermo Fisher Scientific" in Thermofisher.com. https://www.thermofisher.com/be/en/home/life-science/protein-biology/protein-biology-learning-center/protein-biology-resource-library/pierce-protein-methods/carbodiimide-crosslinker-chemistry.html. Consulted on April 28th, 2017.

[32] Gianotti, E., Martins Estevão, B., Cucinotta, F., Hioka, N., Rizzi, M., Renò, F., & Marchese, L. (2014). An efficient rose bengal based nanoplatform for photodynamic therapy. *Chemistry (Weinheim an Der Bergstrasse, Germany)*, *20*(35), 10921–10925.

[33] Lehman, S. E., & Larsen, S. C. (2014). Zeolite and mesoporous silica nanomaterials: greener syntheses, environmental applications and biological toxicity. *Environmental Science: Nano*, *1*(3), 200.

[34] Planas, O., Bresolí-Obach, R., Nos, J., Gallavardin, T., Ruiz-González, R., Agut, M., & Nonell, S. (2015). Synthesis, photophysical characterization, and photoinduced antibacterial activity of methylene blue-loaded amino- and mannose-targeted mesoporous silica nanoparticles. *Molecules*, *20*(4), 6284–6298.

[35] "Cetrimonium bromide" in *En.wikipedia.org.* https://en.wikipedia.org/wiki/Cetrimonium_bromide. Consulted on April 28th, 2017.

[36] "HATU" in *En.wikipedia.org*. https://en.wikipedia.org/wiki/HATU. Consulted on May 5th, 2017.

[37] "Amine to Amide Mechanism – HATU" in *Commonorganicchemistry.com*. http://www.commonorganicchemistry.com/Rxn_Pages/Amine_to_Amide_Coupling/Amine_to_Amide_Coupling_HATU_Mech.htm. Consulted on May 5th, 2017.

[38] Valeur, E., & Bradley, M. (2009). Amide bond formation: beyond the myth of coupling reagents. *Chem Soc Rev*, *38*(2), 606–631.

[39] "Thermogravimetric Analysis (TGA)" in *Us.setaram.com.* http://us.setaram.com/en/product_categories/thermal-analysis/thermogravimetry-tga. Consulted on May 8th, 2017.

[40] "Cleanroom | Grove School of Engineering | City College of New York" in Ees2cy.engr.ccny.cuny.edu. http://ees2cy.engr.ccny.cuny.edu/www/web/sseo/Cleanroom/equip-07.html. Consulted on May 9th, 2017.

[41] “ASAP 2420 | Micromeritics” in *Micromeritics.com*. http://www.micromeritics.com/Product-Showcase/ASAP-2420.aspx. Consulted on May 12th, 2017.

[42] “Thermo Scientific GENESYS 10S UV-Vis Spectrophotometer” in Fishersci.com. https://www.fishersci.com/shop/products/thermo-scientific-genesys-10s-uv-vis-spectrophotometer-10s-uv-vis-single-six-cell/14386515. Consulted on May 22th, 2017.

[43] Pelzer M. (2015). “Développpement d’un microreacteur continu pour le traitement photocatalytique d’effluents liquides”. Master Thesis.

[44] “High Pressure Syringe Pump - Viscous Fluid Syringe Pumps | Chemyx” in Chemyx Inc. https://www.chemyx.com/syringe-pumps/nexus-6000. Consulted on May 23th, 2017.

[45] “Gas Module - FutureChemistry” in FutureChemistry. http://futurechemistry.com/product/gasmodule/. Consulted on May 23th, 2017.

[46] “Products | Zaiput Flow Technologies” in Zaiput.com. http://www.zaiput.com/products. Consulted on May 24th, 2017.

[47] “Back Pressure Regulators | Zaiput Flow Technologies” in Zaiput.com. http://www.zaiput.com/back-pressure-regulators. Consulted on May 24th, 2017.

[48] Yalkowsky, S.H., He, Yan., Handbook of Aqueous Solubility Data: An Extensive Compilation of Aqueous Solubility Data for Organic Compounds Extracted from the AQUASOL dATAbASE. CRC Press LLC, Boca Raton, FL. 2003., p. 175

[49] “L-methionine | C5H11NO2S – PubChem” in Pubchem.ncbi.nlm.nih.gov. https://pubchem.ncbi.nlm.nih.gov/compound/L-methionine#section=Solubility. Consulted on May 24th, 2017.

[50] L-methionine (R)-S-oxide – DrugBank in Drugbank.ca. https://www.drugbank.ca/drugs/DB02235. Consulted on May 24th, 2017.

[51] Robin M. Pope and Edward S. Fry, "Absorption spectrum (380–700 nm) of pure water. II. Integrating cavity measurements," Appl. Opt. 36, 8710-8723 (1997).

[52] “Common Organic Solvents: Table of Properties” in Organicdivision.org. https://www.organicdivision.org/orig/organic_solvents.html. Consulted on May 24th, 2017.

[53] Wilkinson, F., Helman, W. P., & Ross, A. B. (1993). Quantum Yields for the Photosensitized Formation of the Lowest Electronically Excited Singlet State of Molecular Oxygen in Solution. *Journal of Physical and Chemical Reference Data*, *22*(1), 113–262.]

[54] L’homme G.A., “Génie des réacteurs chimiques - Tome 1”. Syllabus, page 102.